

The Heterophilic Snowflake Hypothesis: Training and Empowering GNNs for Heterophilic Graphs

Kun Wang✳️*
wk520529@mail.ustc.edu.cn
University of Science and Technology
of China (USTC)
Hefei, China

Guibin Zhang✳️*
bin2003@tongji.edu.cn
Tongji University
Shanghai, China

Xinnan Zhang
zhan9359@umn.edu
University of Minnesota
Twin Cities, USA

Junfeng Fang
fjf@mail.ustc.edu.cn
University of Science and Technology
of China (USTC)
Hefei, China

Xun Wu
wuxun21@mails.tsinghua.edu.cn
Tsinghua University
Beijing, China

Guohao Li
guohao.li@kaust.edu.sa
Oxford University
Oxford, UK

Shirui Pan
s.pan@griffith.edu.au
Griffith University
Queensland, Australia

Wei Huang†
wei.huang.vr@riken.jp
RIKEN AIP
Tokyo, Japan

Yuxuan Liang†
yuxliang@outlook.com
The Hong Kong University of Science
and Technology (Guangzhou)
Guangzhou, China

ABSTRACT

Graph Neural Networks (GNNs) have become pivotal tools for a range of graph-based learning tasks. Notably, most current GNN architectures operate under the assumption of homophily, whether explicitly or implicitly. While this underlying assumption is frequently adopted, it is not universally applicable, which can result in potential shortcomings in learning effectiveness. In this paper, **for the first time**, we transfer the prevailing concept of “one node one receptive field” to the heterophilic graph. By constructing a proxy label predictor, we enable each node to possess a latent prediction distribution, which assists connected nodes in determining whether they should aggregate their associated neighbors. Ultimately, every node can have its own unique aggregation hop and pattern, much like each snowflake is unique and possesses its own characteristics. Based on observations, we innovatively introduce the Heterophily Snowflake Hypothesis and provide an effective solution to guide and facilitate research on heterophilic graphs and beyond. We conduct comprehensive experiments including (1) main results on 10 graphs with varying heterophily ratios across 10 backbones; (2) scalability on various deep GNN backbones (SGC, JKNet, etc.) across various large number of layers (2,4,6,8,16,32 layers); (3) comparison with conventional snowflake hypothesis; (4) efficiency comparison with existing graph pruning algorithms. Our

observations show that our framework acts as a versatile operator for diverse tasks. It can be integrated into various GNN frameworks, boosting performance in-depth and offering an explainable approach to choosing the optimal network depth. The source code is available at <https://github.com/bingreeky/HeteroSnoH>.

CCS CONCEPTS

• **Computer systems organization** → **Neural networks**; • **Theory of computation** → Sparsification and spanners.

KEYWORDS

Graph Neural Network, Heterophilic Graph, Graph Pruning

ACM Reference Format:

Kun Wang✳️, Guibin Zhang✳️, Xinnan Zhang, Junfeng Fang, Xun Wu, Guohao Li, Shirui Pan, Wei Huang†, and Yuxuan Liang†. 2024. The Heterophilic Snowflake Hypothesis: Training and Empowering GNNs for Heterophilic Graphs. In *Proceedings of the 30th ACM SIGKDD Conference on Knowledge Discovery and Data Mining (KDD '24)*, August 25–29, 2024, Barcelona, Spain. ACM, New York, NY, USA, 19 pages. <https://doi.org/10.1145/3637528.3671791>

1 INTRODUCTION

Graph Neural Networks (GNNs) [21, 27, 63] have become the *de facto* standard for various graph representation learning tasks, such as node classification [2, 49], link prediction [72, 73], and graph classification [19, 69]. The superior capabilities of GNNs can be attributed to their message passing paradigm [63]. Through iterative information aggregation and updating, the central node captures rich information by interacting with its neighboring nodes based on the connected graph structure [51, 63, 76].

Among the various landscape of GNN architectures and designs, the homophily assumption [32, 75, 78] serves as a foundational pillar, suggesting that edges predominantly link nodes with identical labels and analogous node features. Despite its appealing success,

*Kun Wang and Guibin Zhang are co-first authors. † denotes corresponding authors.

Permission to make digital or hard copies of all or part of this work for personal or classroom use is granted without fee provided that copies are not made or distributed for profit or commercial advantage and that copies bear this notice and the full citation on the first page. Copyrights for components of this work owned by others than the author(s) must be honored. Abstracting with credit is permitted. To copy otherwise, or republish, to post on servers or to redistribute to lists, requires prior specific permission and/or a fee. Request permissions from permissions@acm.org.

KDD '24, August 25–29, 2024, Barcelona, Spain

© 2024 Copyright held by the owner/author(s). Publication rights licensed to ACM.

ACM ISBN 979-8-4007-0490-1/24/08...\$15.00

<https://doi.org/10.1145/3637528.3671791>

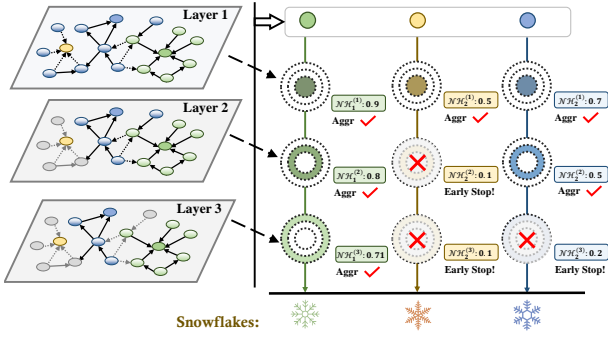


Figure 1: The algorithm workflow of Heterophilic Snowflake Hypothesis (Hetero-S) and Heterophily-aware Early Stopping (HES).

the performance of current GNNs has dropped sharply as the homophily of the graph decreases. Specifically, within heterophilic graphs, a discrepancy is often observed between the labels of neighboring nodes and the central node, a phenomenon referred to as the local structure discrepancy issue [5, 38, 75, 79]. We ascribe the observed performance degradation to the uniform message passing framework, in which that the central node initially aggregates messages from its local neighboring nodes, subsequently updating the ego node (see Figure 1 left hand).

However, non-euclidean data frequently display heterophily, which can be observed across diverse domains. For instance, when users engage with content on Netflix, the people with diverse preferences might be subjected to similar recommendation algorithms, owing to their interaction with identical video content. The potential of heterophilic graphs is vast, holding promise in both academic and industrial spheres, such as social networks [14], transportation systems [56, 77], and recommendation platforms [61, 62]. In a heterophilic context, this mechanism introduces two primary and challenging limitations:

- In graph topology, local neighbors refer to nearby nodes, often overlooking distant yet informative nodes. In heterophilic, nodes sharing structural and semantic characteristics can be more distantly positioned [33, 34].
- A consistent aggregation and update method often neglects variations in information from alike/unalike neighbors. In heterophilic graphs, achieving discerning node representations necessitates customized message passing to capture distinctive patterns.

Given the above emerging challenges, there has been a shifting focus towards exploring heterophily in GNNs. This research area includes a wide range from delving into heterophilic graph sampling to the evolution of intricate algorithms. The growing interest in heterophilic graph learning can be attributed to its vast applicability.

From a macro perspective, existing heterophilic GNNs can be broadly classified into two categories, *i.e.*, **non-local neighbor extension** and **GNN architecture refinement** [75]. The concept of non-local neighbor extension in heterophilic GNNs involves broadening the receptive field beyond local neighbors. This is achieved through strategies like high-order neighbor information mixing [3, 26, 58, 79] and potential neighbor discovery [17, 36, 40, 67], enhancing representation by capturing distant but relevant node features. With the second class, GNN architecture refinement focuses on enhancing the expressive capability of GNNs for heterophilic

graphs by optimizing AGGREGATE and UPDATE function [63]. Through strategies such as adaptive message aggregation [20, 50], ego-neighbor separation [47, 79], and layer-wise operation [7, 9, 65], the refinement aims to produce distinguishable and discriminative node representations.

Recently, a novel paradigm, *the Snowflake Hypothesis* (SnoH) [53], rooted in the concept of “one node, one receptive field” has gained significant attention for its efficacy in addressing the over-smoothing [42] and over-fitting [5, 31] issues in GNNs. This hypothesis draws inspiration from the intricate and distinctive patterns exhibited by individual snowflakes, assuming that each node can possess its unique receptive field. It posits that for an L -layer GNN, every node in the graph harbors an optimal receptive field width denoted as k ($1 \leq k \leq L$). During the message passing process from 1 to L hops, each node merely aggregates information from the preceding k hops, after which they cease to aggregate information from the neighborhood (referred to as “*node early stopping*”).

Intuitively, the snowflake hypothesis demonstrates even greater vitality and significance in the context of heterophilic graphs: (1) **One concept benefits all**. The idea behind the snowflake hypothesis can be seamlessly integrated with any heterophilic GNNs designs, showcasing exceptional versatility. Whether it is for non-local neighbor extension or GNN architecture refinement, the snowflake can easily be incorporated as a plugin and demonstrates strong compatibility. (2) **Enhanced pruning requirement**. In heterophilic graphs, given the higher probability of central nodes having different labels than surrounding nodes, the need for pruning aggregation channels becomes even more critical than in homogeneous graphs. This pruning aids nodes in selectively aggregating information and updating themselves effectively.

However, the original SnoH and its implementations appear to exhibit limitations when applied to heterophilic graphs. Firstly, SnoH relies on either *gradient information* or *cosine similarity* comparison for node early stopping. These heterophily-unaware approaches do not adequately integrate into heterophilic scenarios. Secondly, SnoH typically demonstrates convincing performance only in deep GNNs, which contradicts the prevailing focus on shallow designs for heterophilic GNNs. These necessitates bespoke strategies for heterophilic graphs. To handle the distinct characteristics between homophilic and heterophilic graphs, we introduce a **Heterophily-aware Early Stopping (HES)** strategy. HES benefits from two key aspects, thereby overcoming the limitations of SnoH:

- HES employs a proxy label predictor, generating pseudo-label probability distributions for different nodes [11, 22]. In this way, we can scrutinize the probability distributions of two connected nodes and determine the probabilities where two nodes are predicted to have the same label. This value can further represent the homophily score between two nodes, subsequently serving as a replacement for the original adjacent matrix.
- By analyzing the variation in the heterophilic ratio across each layer, we are able to appropriately determine the depth for early stopping. This approach contrasts with SnoH, which primarily exhibits efficacy in deeper GNN configurations.

Subsequently, by determining whether the heterophily of nodes increases before and after aggregation, we implement early stopping at the node receptive field level, thereby ensuring the efficacy

of information aggregation. **For the first time**, we validate the existence of “snowflakes” in heterophilic graphs, underscoring the significance of the “one node, one receptive field” paradigm in such scenarios. We introduce a universal solution to this issue, which stands out from previous designs due to its generality and model-agnostic nature. Remarkably, HES can **seamlessly** integrate with virtually **arbitrary** heterophilic designs, enhancing both its training and inference speeds. We summarize our contributions as follows:

- We conceptualize “one node one receptive field” as heterophilic snowflake hypothesis in the heterophilic graph scenario. To achieve this target, we develop the heterophily-aware early stopping strategy, and offer theoretical analysis from the graph neural tangent kernel (GNTK) and stochastic block model (SBM) perspective to provide high-level insights of ours paradigm.
- Hetero-S finds broad applicability and HES can aid various backbones in discovering optimal receptive fields for each node across diverse datasets. We verify HES on 10 GNN backbones across over 16 graph benchmarks. Experiments demonstrate that for all prevailing backbones, HES can facilitate substantial performance enhancements, ranging from 0.34% ~ 31.86% in homophilic settings and from 0.68% ~ 21.73% in heterophilic settings.
- Similar to the conventional snowflake hypothesis, HES can scale up to deep GNNs effectively without any bells and whistles. Concretely, HES mitigates the performance degradation caused by excessive aggregation of heterophilic information, resulting in performance improvements ranging from 0.46% ~ 10.37% in 16-layer configurations and from 1.13% ~ 7.92% in 32-layer configurations. These experimental results demonstrate the potential of HES to be extended to large and densely connected graphs.
- **More observations.** (I) Hetero-S has been empirically observed to exhibit comparable or even superior performance to the original snowflake hypothesis on both homophilic and heterophilic settings. In particular, Hetero-S demonstrates performance improvements ranging from 0.51% ~ 8.44% on MixHop and JKNet in comparison to SnoH. (II) The **snowflakes** (⊙) achieves the highest multiply-accumulate operations (MACs) saving (25% ~ 45% of the baseline) compared to SOTA graph pruning algorithms [8, 37], without any performance compromise.

2 PRELIMINARIES

2.1 Notations

We consider an attributed graph denoted as $\mathcal{G} = \{\mathcal{V}, \mathcal{E}\}$, where \mathcal{V} and \mathcal{E} represent the sets of nodes and edges, respectively. The feature matrix of \mathcal{G} is denoted as $\mathbf{X} \in \mathbb{R}^{N \times D}$, where $N = |\mathcal{V}|$ is the number of nodes in the graph and D is the dimension of node features. We use $\mathbf{x}_i = \mathbf{X}[i, \cdot]$ to denote the D -dimensional feature vector corresponding to node $v_i \in \mathcal{V}$. An adjacency matrix $\mathbf{A} \in \mathbb{R}^{N \times N}$, serves to represent the connections between nodes, where $\mathbf{A}[i, j] = 1$ if $(v_i, v_j) \in \mathcal{E}$ and 0 otherwise. To learn the node representations in a graph \mathcal{G} , most GNNs adhere to the following paradigm of neighborhood aggregation and message passing:

$$\mathbf{h}_i^{(l)} = \text{COMB} \left(\mathbf{h}_i^{(l-1)}, \text{AGGR} \{ \mathbf{h}_j^{(k-1)} : v_j \in \mathcal{N}(v_i) \} \right), \quad 0 \leq l \leq L \quad (1)$$

where L is the number of GNN layers, $\mathbf{h}_i^{(0)} = \mathbf{x}_i$ denotes the feature vector of v_i and $\mathbf{h}_i^{(l)}$ ($1 \leq l \leq L$) denotes the node embedding

of v_i at the l -th GNN layer. **AGGR** and **COMB** represent functions used for aggregating neighborhood information and combining ego- and neighbor-representations, respectively. In the general node classification setting, after the graph convolution operations, GNN uses a linear mapping to map the node embedding $\mathbf{h}_i^{(l)}$ to the corresponding prediction probability value \mathbf{z}_i , and eventually get the model prediction \hat{y}_i :

$$\mathbf{z}_i = \text{softmax}(\mathbf{h}_i^{(l)} \mathbf{W}), \quad \text{and} \quad \hat{y}_i = \arg \max \{ \mathbf{z}_i \}, \quad (2)$$

where \mathbf{W} is a learnable matrix, $\mathbf{z}_i \in \mathbb{R}^C$ signifies the probabilities of categorizing v_i into each of the C categories.

2.2 Heterophily in Graph Neural Networks

Following the previous heterophilic GNNs [40], we define the node- and graph-level homophily ratio as follows:

$$\text{node-level: } \mathcal{H}_{\text{node}}^{(i)} = \frac{|\{v_j | v_j \in \mathcal{N}(v_i), y_i = y_j\}|}{|\mathcal{N}(v_i)|}, \quad (3)$$

$$\text{graph-level: } \mathcal{H}_{\text{node}} = \frac{1}{|\mathcal{V}|} \sum_{v_i \in \mathcal{V}} \mathcal{H}_{\text{node}}^{(i)}, \quad (4)$$

where $\mathcal{N}(v_i)$ denotes the 1-hop neighbor of v_i and $\mathcal{V}(v_i)$ denotes the 1-hop neighbors of v_i . Specifically, $\mathcal{H}_{\text{node}}^{(i)}$ represents the average proportion of neighbors that share the same class with node v_i , and $\mathcal{H}_{\text{node}}$ represents the global homophily by computing the average of node homophily. Conversely, the heterophily ratio at the node and graph level can be expressed as $\tilde{\mathcal{H}}_{\text{node}}^{(i)} = 1 - \mathcal{H}_{\text{node}}^{(i)}$ and $\tilde{\mathcal{H}}_{\text{node}} = 1 - \mathcal{H}_{\text{node}}$. In general, graphs that exhibit strong homophily tend to have $\mathcal{H}_{\text{node}}$ values approaching 1, whereas those characterized by pronounced heterophily often have values near 0.

It’s essential to note that $\mathcal{H}_{\text{node}}^{(i)}$ solely reflects the heterophily within the 1-hop neighborhood of v_i . Furthermore, we extend this definition to the k -hop neighborhood:

$$\mathcal{NH}_i^k = \frac{|\{v_j | v_j \in \mathcal{N}^{(k)}(v_i), y_i = y_j\}|}{|\mathcal{N}^{(k)}(v_i)|}, \quad (5)$$

where $\mathcal{N}^{(k)}(v_i) = \{v_j | 1 \leq \text{ShortestPath}(v_j, v_i) \leq k\}$ represents the k -hop neighborhood of v_i .

3 MOTIVATION

In this section, we prudently introspect the heterophily in different graphs and put forward the motivation of HES strategy. We start from the empirical observations. Concretely, we select both a heterophilic graph (Squirrel) and a homophilic graph (CS), and compute \mathcal{NH}_i^k ($1 \leq k \leq 6$) for each node. As shown in Figure 2 (a,b), we list the following two observations: **Obs.1:** The homophily ratio of nodes in Squirrel significantly declines as the hop increases at a faster rate compared to those in CS; **Obs.2:** In both types of graphs, the distribution of node homophily ratios is diverse. Even when the receptive field size extends to 6 layers (*i.e.*, 6-hop neighborhood), there exist nodes with homophily ratios approaching 1.

Insights & Reflections. These observations naturally align with the concept of “one node one receptive field.” In both types of graph data, the k -hop homophily distributions of different nodes exhibit significant variation. This prompts the question: *Is it feasible to*

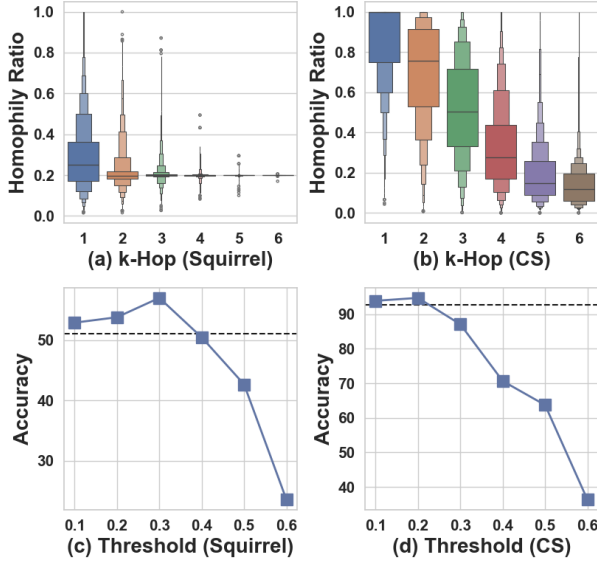


Figure 2: The algorithm workflow of Heterophilic Snowflake Hypothesis (Hetero-S) and Heterophily-aware Early Stopping (HES).

determine the appropriate receptive field for each node based on its k -hop homophily distribution? Going beyond this insight, we conduct the **empirical experiments** on Squirrel and CS with a 6-layer GNN. We determine their receptive field as follows:

$$\mathcal{R}_i = \max_{1 \leq j \leq k} (j \cdot \mathbb{1}[\mathcal{NH}_i^j \leq \epsilon]), \quad (6)$$

where \mathcal{R}_i denotes the determined receptive field for v_i and ϵ is a pre-defined homophily threshold. After obtaining the receptive field, we then reformulate the aggregation operations as follows:

$$\mathbf{h}_i^{(l)} = \begin{cases} \text{COMB}(\mathbf{h}_i^{(l-1)}, \text{AGGR}\{\mathbf{h}_j^{(k-1)} : v_j \in \mathcal{N}(v_i)\}), & 0 \leq l < \mathcal{R}_i; \\ \text{COMB}(\mathbf{h}_i^{(l-1)}, \emptyset), & \mathcal{R}_i \leq l \leq L \end{cases} \quad (7)$$

It is noteworthy that, beyond the \mathcal{R}_i -th layer of GNN, node v_i ceases to aggregate information from its neighbors, thus achieving early stopping of the receptive field. Further, Figure 2 (c,d) demonstrates the performance of GCN on Squirrel and CS with different homophily thresholds, which characterizes a 2.12% \uparrow under $\epsilon = 0.3$ on Squirrel, and a 1.34% \uparrow under $\epsilon = 0.2$ on CS. This confirms that early stopping of node receptive fields can indeed assist GNNs in learning more refined node representations.

4 METHODOLOGY

Considering the aforementioned observation and gained motivations, we aim to identify an appropriate receptive field for each node. Analogous to the conventional snowflake hypothesis, we introduce the ‘‘Heterophily Snowflake Hypothesis (Hetero-S)’’ for the first time in heterophilic graphs settings:

Heterophilic Snowflake Hypothesis (Hetero-S): For an L -layer GNN on a heterophilic graph, each node possesses an optimal receptive field; training the GNN by aggregating information only from neighbors within this optimal receptive field minimizes the inclusion of excessive heterophilic information, yielding optimal representations.

More formally, consider an L -layer GNN, when optimized with stochastic gradient descent (SGD) on heterophilic graphs $\mathcal{G} = \{\mathbf{A}, \mathbf{X}\}$, the GNN reaches a minimum validation loss and obtains a test accuracy of φ . Furthermore, let’s assume the existence of a pruning algorithm guided by the $\mathcal{H}_{\text{node}}$, which ensures that each node v_i has a unique optimal receptive field size of $k_i (1 \leq k_i \leq L)$, allowing it to be early stopped at the k_i -th GNN layer, *i.e.*, set $\mathcal{N}^{(k+1)}(v_i) = \dots = \mathcal{N}^{(L)}(v_i) = \emptyset$. This approach helps nodes avoid over-aggregation of heterophilic information, leading to a test accuracy of φ' . The Hetero-S posits that there exists optimal k_i for each v_i to satisfy that $\varphi' > \varphi$ (note as \ast).

To achieve this target, we can naturally resort to the implementation in Sec. 3. However, in practical scenarios (*e.g.*, semi-supervised settings), a question arises regarding receptive field operation: *when only partial nodes have known labels, how can we estimate the homophily ratio for each node within a k -hop neighborhood?*

4.1 Proxy Label Predictor

As depicted above, in semi-supervised scenarios, we only know a small fraction of labels in a heterophilic graph. Towards this end, we formulate a GNN prediction process as a combination of two processes, *i.e.*, $Y = \{\text{AGGR} \diamond \text{COMB}\} \diamond f_Y$. After the aggregation and combination process, $\{\text{AGGR} \diamond \text{COMB}\}$, nodes are mapped into a latent space characterized by distinguishability. This mapping ensures that nodes with the same label are positioned in similar locations, facilitating the identification of their relational patterns. Moreover, by employing an oracle function, we can effectively predict the outcome Y , leveraging the structured information encapsulated in this latent space. This process enhances the model’s ability to discern and categorize nodes, significantly improving the accuracy and efficiency of our predictions. Upon reviewing previous work [39], we first present a lemma:

LEMMA 4.1. Assuming that \mathcal{NH}_i^k for v_i decreases w.r.t k in proportion to ζ ($\zeta > 1$), meaning that as the receptive field expands, v_i aggregates more heterophilic information. Under such circumstances, when employing receptive field stopping, there exists $k \geq 2$ satisfying the condition that $\varphi(\{\text{AGGR} \diamond \text{COMB}\}^{(k)} \diamond f_Y) > \varphi(\{\text{AGGR} \diamond \text{COMB}\}^{(k+\pi)} \diamond f_Y)$, where $\varphi(\cdot)$ is the performance metric, $\{\text{AGGR} \diamond \text{COMB}\}^{(k)}$ signifies aggregating information solely from the k -hop neighborhood, and $\pi \in \mathbb{N}^+$.

With this in mind, we construct a proxy label predictor \mathcal{P}_Y to determine label-wise graph aggregation [11, 22]. Concretely, we resort to a simple predictive model (here we can use MLP and GNN, and we place ablation results in Sec. 5.5) to obtain pseudo probability label \tilde{z}_i with cross-entropy loss:

$$\min_{\Theta} \mathcal{L}_{\text{CE}}(\mathcal{G}_{tr}, \Theta) = -\frac{1}{|\mathcal{V}_{tr}|} \sum_{v_i \in \mathcal{V}_{tr}} \tilde{z}_i \log(z_i), \quad (8)$$

where \mathcal{G}_{tr} denotes the training nodes (\mathcal{V}_{tr}) and graph structure, and Θ denotes network parameters. Different from previous work [11, 22, 52], we derive a pseudo probability distribution solely to determine the appropriate size of the receptive field.

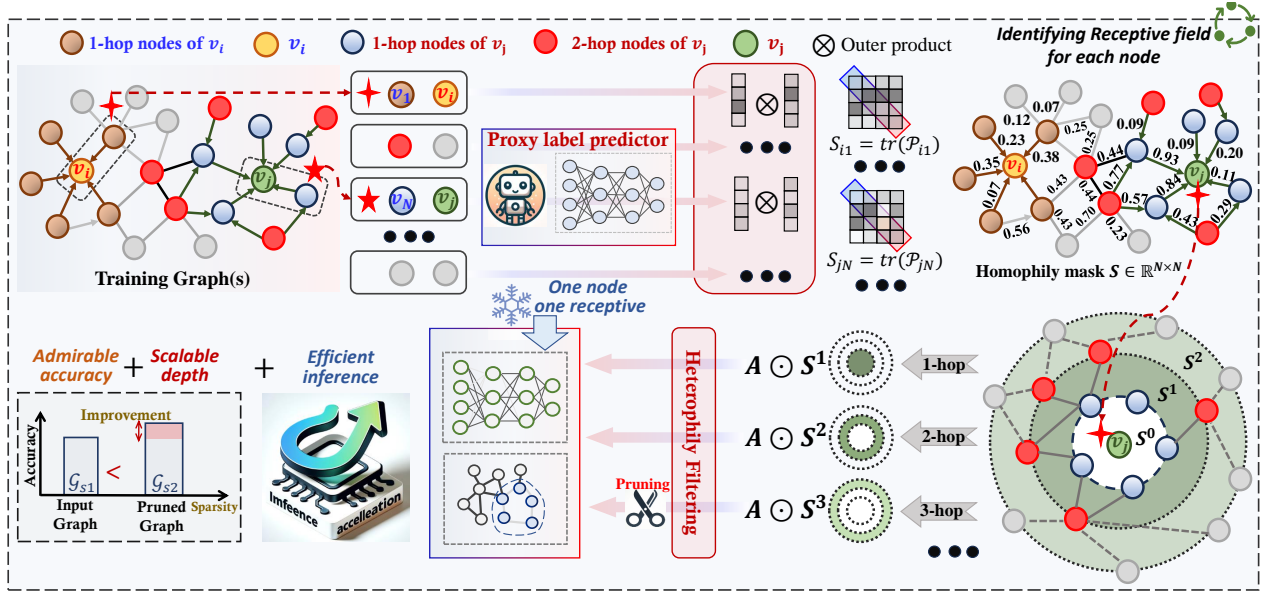


Figure 3: The pipeline of our HES framework. For each node, we utilize a proxy model to evaluate the homophily strength of its edges, which is further used to estimate its multi-hop homophily ratio. Based on the homophily strength at each hop, we perform receptive field-level early stopping to determine a unique receptive field for each node.

4.2 Training Homophily Mask

After obtaining the node soft labels, we proceed to define the *homophily mask* denoted as S , where S_{ij} , for edge $(i, j) \in \mathcal{E}$, represents the homophily strength of edge (i, j) , i.e., the likelihood that v_i and v_j share the same label.

To obtain the expression for S_{ij} , we calculate the label distribution for nodes v_i and v_j by computing the outer product of their respective predicted probability distributions.

$$S_{ij} = \text{tr}(\tilde{z}_i \otimes \tilde{z}_j) = \text{tr} \begin{pmatrix} \tilde{z}_{i,1} & \cdots & \tilde{z}_{i,C} \\ \vdots & \ddots & \vdots \\ \tilde{z}_{C,1} & \cdots & \tilde{z}_{C,C} \end{pmatrix} = \sum_{\mu=1 \rightarrow C} \tilde{z}_{\mu,\mu} \quad (9)$$

where $\tilde{z}_{\alpha,\beta}$ denotes the probability that node v_i belong to category α , while node v_j is associated with category β . \otimes represents the out-product. Then we can formulate the S via following equation:

$$S = \begin{pmatrix} S_{1,1} & \cdots & S_{1,N} \\ \vdots & \ddots & \vdots \\ S_{N,1} & \cdots & S_{N,N} \end{pmatrix} \quad (10)$$

Note that S is parameterized by the proxy model \mathcal{P}_Y . The shapes of S and A are identical, in which we can co-optimize the weight Θ and the S from end to end by utilizing objective \mathcal{L}_{opt} :

$$\mathcal{L}_{\text{opt}} = \mathcal{L}_{\text{CE}}(\{S \odot A, X\}, \Theta) = \mathcal{L}_{\text{CE}} \left(\left\{ \text{opt}_S \left\{ \min_{\Theta_{tr}} \mathcal{G}_{tr}(\mathcal{P}_Y) \right\} \odot A, X \right\}; \Theta \right) \quad (11)$$

where \mathcal{L}_{CE} denotes cross-entropy loss, we optimize (opt) S by function $\text{opt}_S \left\{ \min_{\Theta_{tr}} \mathbb{E}_{\mathcal{G}_{tr}}(\mathcal{R}_Y) \right\}$ with minimized empirical risk \mathbb{E} .

4.3 Early Stopping Based on Hop Heterophily

After multiple rounds of training and optimization with Equation 11, we obtain a relatively accurate mask, denoted as \hat{S} . In the context of GNNs, multi-layer aggregation assists the model in capturing neighbor relationships at varying distances. Here, we employ \hat{S} to replace A for capturing more distant neighbor relationships. Concretely, we use $\hat{S}^{(k)} = \hat{S}^k \in \mathbb{R}^{N \times N}$ to further represent the k -hop neighbor aggregation expression of homophily ratio. Subsequently, we calculate the row sum values for each hop, excluding self-loops:

$$\text{set} \left\{ \sum_{\text{row} \setminus \text{diag}} \hat{S}^{(k)} \right\} = \{ \hat{S}_1^{(k)}, \hat{S}_2^{(k)} \dots \hat{S}_N^{(k)} \}, \quad (12)$$

where $\hat{S}_i^{(k)}$ represents the normalized row sum of the i -th row in $\hat{S}^{(k)}$, where the summation excludes the self-loop represented by row $\{k, k\}$ in the k -th row of the matrix.

$$\text{if } \hat{S}_i^{(k)} > \rho \hat{S}_i^{(ES)} \\ \text{then } \mathcal{D}_o \left(\mathcal{N}^{(ES)}(v_i) = \mathcal{N}^{(ES+1)}(v_i) = \dots = \emptyset \right), \quad (13)$$

where ρ denotes the filtering threshold. While it is possible to assign a distinct threshold for each node, for simplicity, we employ a uniform ρ across all nodes to filter the receptive field (the sensitivity analysis on ρ is placed in Appendix G). \mathcal{D}_o denotes an intervention that forcefully assigns an aggregation status. We employ heterophily-aware early stopping at ES -th layer, which can ensure that each node possesses a unique receptive field size.

4.4 Theoretical Analysis

We provide a theoretical guarantee for heterophily snowflake hypothesis through graph neural tangent kernel (GNTK) [12, 23]. Generally, during training, the NTK is deterministic and static [24], thus GNTK can be used to describe the training behavior of an

infinitely-wide graph neural network. In this work, we use GNTK to study the *training dynamics* of an infinitely-wide GNN with node classification task. We provide the definition of GNKT as follows:

$$K(u, u') = \sum_{l=1}^L \frac{\partial f(u)}{\partial \theta^{(l)}} \frac{\partial f(u')}{\partial \theta^{(l)}} \triangleq \sum_{l=1}^L K(u, u')^{(l)} \quad (14)$$

where u and u' are indexes of nodes in the graph, and $\theta^{(l)}$ is the set of all trainable parameters in l -th layer. According to Equation (14), we need to calculate the GNTK at each layer, which follows the recursive relation: $\mathbf{K}^{(l)} = \mathbf{G}^{(l)} \mathbf{K}^{(l-1)}$, where $\mathbf{G}^{(l)} = \hat{\mathbf{A}}^{(l)} \Gamma(\hat{\mathbf{A}}^{(l)})$ is l -th layer propagation matrix for the GNTK with $\hat{\mathbf{A}} = \mathbf{D}^{-1} \mathbf{A}$, Γ denotes the transpose operation. Our target is to check if the smallest eigenvalue of GNTK is greater than zero or not. **According to [22], when the smallest eigenvalue of GNTK is greater than zero, the training loss can be minimized to zero, implying successful optimization.** Inversely, if the smallest eigenvalue of is zero, then we would say that the GNN cannot be trained successfully. To study the eigenvalue of GNTK, we introduce a generative model named Stochastic Block Model (SBM) [1, 18], which has been used in the theoretical analysis of GNNs. Then the following Lemma gives the smallest eigenvalue of the GNTK:

LEMMA 4.2. *Consider \mathbf{A} is a probability adjacency matrix sampled from a SBM $\psi(N, p, q)$, wherein it is postulated that there are various clusters interconnected with an internal connection probability of p , and the inter-cluster connectivity rate is q . We can conclude the expected smallest eigenvalue of the GNTK is given by $\mathbb{E}_{\mathbf{A} \sim \psi(N, p, q)}[\lambda] = \prod_{i=1}^L \frac{1-p}{(N-1)p+Nq+1}$.*

In SBM, p and q can be deemed as the expectation of the adjacency matrix. With this in mind, we observe the $\mathbf{K}^{(l)} = \mathbf{G}^{(l)} \mathbf{K}^{(l-1)} = \dots = \mathbf{G}^{(l)} \dots \mathbf{G}^{(1)} \mathbf{K}^{(0)}$. Subsequently, we can express the general probabilistic form of $\mathbf{K}^{(l)}$:

$$\mathbf{K}^{(l)} = \hat{\mathbf{A}}^{(l)} \Gamma(\hat{\mathbf{A}}^{(l)}) \hat{\mathbf{A}}^{(l-1)} \Gamma(\hat{\mathbf{A}}^{(l-1)}) \dots \hat{\mathbf{A}}^{(1)} \Gamma(\hat{\mathbf{A}}^{(1)}) \mathbf{K}^{(0)} \quad (15)$$

where l -th adjacency matrix $\hat{\mathbf{A}}^{(l)}$ is further characterized in probabilistic form, and the density of $\hat{\mathbf{A}}^{(l)}$ is correlated with the magnitude of $p^{(l)}$ and $q^{(l)}$. We observe that with the increasing depth of GNN, early stopping of the receptive field can assist in the hierarchical decrement of p and q . Consider a simple binary classification scenario with a balanced distribution, where each category consists of N nodes. The eigenvalues of matrix $\mathbb{E}_{\mathbf{A} \sim \psi(N, p, q)}[\mathbf{G}]$ are as follows:

$$\lambda_0 = 1, \lambda_1 = \frac{(N-1)p - Nq + 1}{(N-1)p + Nq + 1}, \lambda_2 = \dots = \lambda_{2N-1} = \frac{1-p}{(N-1)p + Nq + 1} \quad (16)$$

Generally, the probability of connection between nodes with the same class label is higher than that of different classes, *i.e.*, $p > q$. Hence, the inequality $(1-p) < (N-1)p - Nq + 1$ is always satisfied. Therefore, the smallest eigenvalue of the SBM is given by $\frac{1-p}{(N-1)p+Nq+1}$. Considering in subsequent layers, the HES algorithm is applied such that p and q remain attenuation while heterophilic nodes are pruned (the decay rate of p is slower), the product of the smallest eigenvalues is given by:

$$\prod_{i=1}^L \frac{1-p^{(i)}}{(N-1)p^{(i)} + Nq^{(i)} + 1} = \prod_{i=1}^L \left(1 - \frac{N(p^{(i)} + q^{(i)})}{(1-p^{(i)}) + N(p^{(i)} + q^{(i)})} \right) \quad (17)$$

Consider $p > q$ and p, q are both functions of N . Here, we conduct a case study where both p and q decay quadratically with i . Without loss of generality, we assume $p = 1/((N-1)*i^2)$ and $q = 1/(N*i^2)$. We observe that, under these conditions, the GNTK eventually diverges to $\sqrt{2N} \operatorname{csch}(\sqrt{2}\pi) \sin(\pi/\sqrt{N})$, which concludes the proof. See details in Appendix J.

5 EXPERIMENTS

In this section, we conduct extensive experiments to answer the following research questions (RQ):

- **RQ1.** Can Hetero-S boost the performance of prevailing homophilic & heterophilic GNNs on heterophilic graphs?
- **RQ2.** Does Hetero-S facilitate heterophilic GNNs to extend to more deep network structures?
- **RQ3.** Can Hetero-S genuinely achieve graph sparsity and accelerate computations compared to mainstream graph pruning algorithms [4, 8, 15, 16, 30]?
- **RQ4.** How sensitive is Hetero-S to its key components?

To provide answers to these questions, we orchestrate the experiments including **Main experiments**, **Depth scalability experiments**, **Comparative analysis with traditional Snowflake Hypotheses (SnoH)** and **Efficiency comparison with pruning algorithms** four parts. Detailed descriptions can be found in Appendix C. Through these experiments, we anticipate drawing clear conclusions regarding the efficacy of Hetero-S.

5.1 Experiment Setup

Datasets. We verify Hetero-S across 10 graph benchmarks, including citation networks: Cora, CiteSeer, and PubMed [27]; WebKB networks: Cornell, Texas, and Wisconsin [40]; Wikipedia-derived networks: Chameleon and Squirrel [44]; the actor co-occurrence network Actor [40]; the heterogenous information network DBLP [57]. Table 4 in Appendix A offers a comprehensive overview of dataset details. Note that we choose both highly homophily graphs with $\mathcal{H}_{\text{node}} > 0.8$ and heterophilic graphs with $\mathcal{H}_{\text{node}} > 0.1$.

Backbones. We select three categories of GNN designs, including the *non-local neighbor extension*, *GNN architecture refinement* as stated in Section 1, along with some general GNN backbones. Specifically, for non-local neighbor extension, we choose Mixhop [3] and GPNN [67]. For GNN architecture refinement designs, we opt for backbones like GAT [50], H2GCN [79], GCNII [7], GeomGCN [40], JKNet [65], and MGNN [10]. Lastly, we choose some general-purpose GNNs, such as GCN [27] and GIN [64], to further validate the universality of our algorithm.

5.2 Main Results (RQ1)

We initially investigate the presence and identifiability of the heterophily snowflake hypothesis (Hetero-S) through the heterophily-aware early stopping (HES) mechanism. We evaluate HES in conjunction with selected GNN backbones across 10 graph benchmarks. Our tests span not only the standard homophilic datasets but also extend to heterophilic graphs. From the Table 1 and Figure 4, we list the following **Observations**:

Obs.1. The snowflake (❄️) broadly exist under 2 ~ 8 layer backbones settings. As shown in Table 1, upon implementing the HES algorithm, the model consistently achieved performance improvements. For instance, under the MGNN+Cora setup, the model at 8

Table 1: Quantitative performance for different layers, we report the average results of FIVE runs and record the results after adding Hetero-S (+*). “8*” in 🏆 column denotes 8-th layer GNN with HES shows the best performance. OOM represents out-of-memory.

Layers	2	4	6	8	🏆	2	4	6	8	🏆	2	4	6	8	🏆
Cora ($\mathcal{H}_{node} = 0.57$)															
GCN/ +*	81.60	82.10/82.73	83.20/84.00	83.90/85.10	8*	72.80	73.20/73.40	73.80/73.40	73.20/74.20	8*	87.70	87.90/88.50	87.40/88.12	87.50/87.98	4*
GIN/ +*	73.60	78.30/79.70	81.10/81.30	78.80/82.10	8*	60.51	68.47/72.96	73.08/73.50	72.60/74.50	8*	87.60	86.37/88.18	88.51/89.37	88.45/88.70	6*
GAT/ +*	82.70	83.52/84.28	85.31/85.42	83.40/85.19	6*	73.78	75.15/75.98	74.21/74.30	74.15/73.80	4*	87.40	85.12/85.52	85.10/85.50	84.32/85.08	2
Mixhop/ +*	85.20	82.80/84.07	82.10/82.80	82.16/83.90	2	76.98	75.90/77.25	75.50/77.88	74.30/77.10	6*	77.20	77.30/77.40	75.70/76.70	73.20/77.28	4*
Geom-GCN/ +*	85.35	21.02/86.77	19.42/81.24	14.67/78.99	4*	78.42	29.98/67.43	25.66/68.47	12.04/64.26	2	85.95	73.22/87.03	43.66/80.38	40.58/74.63	4*
H2GCN/ +*	77.05	75.74/76.52	87.14/87.83	85.76/87.98	8*	78.02	76.42/78.25	75.64/78.18	75.46/78.24	8*	88.54	87.74/88.66	86.02/88.72	85.28/88.52	6*
GCNII/ +*	84.40	79.50/84.85	76.30/81.50	47.90/73.60	4*	74.60	73.32/72.89	71.70/72.66	54.79/57.99	2	86.50	85.57/87.25	84.00/84.92	82.53/84.60	4*
GPNN/ +*	81.20	80.73/82.80	73.43/78.99	46.49/62.18	4*	74.20	73.30/74.81	73.80/74.38	72.50/73.64	4*	88.66	89.45/89.71	40.70/88.19	40.70/85.10	4*
JKNet/ +*	83.00	82.51/83.37	80.50/83.19	81.60/83.39	4*	74.19	73.28/74.42	72.60/73.88	73.10/74.05	4*	88.78	88.20/89.41	88.78/88.06	87.70/88.90	4*
MGNN/ +*	66.80	63.60/74.72	73.81/75.27	79.30/84.88	8*	43.90	53.30/70.46	69.50/78.33	77.08/79.30	8*	89.20	90.07/90.20	88.80/89.47	88.27/89.16	4*
Texas ($\mathcal{H}_{node} = 0.11$)															
GCN/ +*	68.42	73.68/78.95	68.42/71.05	60.53/63.16	4*	56.86	41.48/50.98	47.06/60.78	52.94/54.90	6*	36.84	34.21/44.74	39.47/47.37	34.21/39.47	6*
GIN/ +*	63.16	71.02/76.32	73.68/76.32	77.84/78.85	8*	62.75	45.10/54.08	54.88/58.82	52.17/62.84	8*	34.21	28.95/36.27	26.77/38.42	36.84/37.20	6*
GAT/ +*	60.53	60.53/65.79	57.89/65.79	60.53/63.16	6*	52.94	51.79/54.90	49.62/56.86	50.26/54.33	6*	36.84	31.58/39.76	26.32/34.21	26.38/36.84	4*
Mixhop/ +*	92.11	89.47/94.86	86.44/89.68	78.95/76.32	4*	80.39	82.35/84.31	74.51/82.93	68.63/80.28	4*	73.68	52.63/68.99	50.80/64.32	39.47/65.70	2
Geom-GCN/ +*	66.53	60.84/66.98	43.17/60.34	43.08/58.26	4*	64.51	61.88/66.92	36.87/54.22	36.87/55.92	4*	60.54	24.78/48.99	24.78/52.96	24.78/46.71	2
H2GCN/ +*	89.54	68.52/92.02	73.43/92.28	73.78/89.26	6*	76.42	72.75/78.23	63.73/76.41	72.48/78.62	8*	55.76	65.45/69.52	65.24/63.02	44.62/57.46	4*
GCNII/ +*	72.68	71.65/73.68	65.79/68.73	63.16/63.89	4*	45.10	49.02/51.38	45.77/49.86	42.71/45.10	4*	73.68	52.63/68.49	50.00/69.72	39.47/66.10	2
GPNN/ +*	78.95	60.53/84.21	60.53/83.18	73.66/78.06	4*	66.67	70.59/71.28	72.35/70.16	68.39/76.91	8*	50.00	52.83/63.24	50.06/49.66	49.72/52.47	4*
JKNet/ +*	74.89	78.95/84.21	84.07/84.30	84.07/89.88	8*	47.60	60.38/62.94	60.38/64.99	56.17/63.82	6*	34.21	42.17/47.25	43.66/50.07	44.89/48.65	6*
MGNN/ +*	84.21	86.84/92.31	88.37/89.64	84.21/93.09	8*	72.55	84.31/86.27	82.35/88.77	80.17/86.20	6*	55.26	68.18/71.22	65.99/71.08	65.03/70.83	4*
Wisconsin ($\mathcal{H}_{node} = 0.21$)															
GCN/ +*	67.11	63.82/63.39	59.65/63.38	57.89/60.31	2	63.82	62.28/66.89	60.31/64.04	58.11/61.62	4*	29.98	26.64/25.67	27.50/28.60	26.83/28.22	2
GIN/ +*	66.89	54.39/54.69	44.36/48.46	46.49/29.77	2	66.89	54.39/54.69	44.36/48.46	46.49/29.77	2	31.84	24.61/24.67	24.93/26.85	24.47/24.80	2
GAT/ +*	69.74	70.61/70.83	66.89/66.23	61.84/63.77	4*	69.74	70.61/70.83	66.89/66.23	61.84/63.77	4*	28.09	27.57/27.87	25.26/25.86	25.13/26.58	2
Mixhop/ +*	66.45	64.69/69.08	63.38/66.04	62.67/65.89	4*	66.45	64.69/69.08	63.38/66.04	62.67/65.89	4*	32.63	31.25/34.80	35.72/36.68	35.20/35.28	6*
Geom-GCN/ +*	38.44	36.47/40.33	31.42/38.67	27.00/36.92	4*	60.75	61.42/63.92	55.73/59.12	54.32/58.46	4*	31.59	22.64/32.26	22.64/33.40	22.64/28.21	6*
H2GCN/ +*	27.35	27.94/27.04	30.07/28.21	OOM	6*	55.86	55.92/53.82	53.07/55.24	51.24/56.04	8*	33.24	32.66/33.74	33.58/33.35	33.02/33.47	4*
GCNII/ +*	40.61	37.94/43.99	33.24/30.58	28.43/29.66	4*	66.89	54.39/54.69	44.36/48.46	46.49/29.77	2	31.84	24.61/24.67	24.93/26.85	24.47/24.80	2
GPNN/ +*	43.04	27.95/38.74	18.54/29.47	18.54/28.61	2	64.47	50.66/65.55	48.03/52.77	29.39/45.08	4*	24.67	25.00/25.63	24.67/24.88	22.18/25.09	4*
JKNet/ +*	47.36	59.75/61.08	58.69/61.22	57.83/61.48	8*	64.25	70.18/72.37	70.83/69.44	70.61/70.93	4*	28.09	27.17/29.67	27.57/30.04	28.09/29.65	6*
MGNN/ +*	41.79	45.44/48.76	41.31/43.79	39.00/40.28	4*	58.33	64.25/64.79	61.18/62.80	61.40/59.72	4*	30.53	35.99/37.65	35.92/37.23	37.17/37.08	4*
Squirrel ($\mathcal{H}_{node} = 0.22$)															
GCN/ +*	55.83	53.51/56.20	51.01/51.87	49.76/53.74	4*	67.11	63.82/63.39	59.65/63.38	57.89/60.31	2	29.98	26.64/25.67	27.50/28.60	26.83/28.22	2
GIN/ +*	46.69	43.26/47.93	43.23/46.89	39.48/44.86	4*	63.82	62.28/66.89	60.31/64.04	58.11/61.62	4*	29.34	29.87/30.83	23.95/25.46	24.41/25.68	4*
GAT/ +*	60.42	46.11/47.55	19.31/28.41	21.33/26.33	2	69.74	70.61/70.83	66.89/66.23	61.84/63.77	4*	28.09	27.57/27.87	25.26/25.86	25.13/26.58	2
Mixhop/ +*	54.76	56.20/56.88	54.84/53.67	52.55/52.87	4*	66.45	64.69/69.08	63.38/66.04	62.67/65.89	4*	32.63	31.25/34.80	35.72/36.68	35.20/35.28	6*
Geom-GCN/ +*	38.44	36.47/40.33	31.42/38.67	27.00/36.92	4*	60.75	61.42/63.92	55.73/59.12	54.32/58.46	4*	31.59	22.64/32.26	22.64/33.40	22.64/28.21	6*
H2GCN/ +*	27.35	27.94/27.04	30.07/28.21	OOM	6*	55.86	55.92/53.82	53.07/55.24	51.24/56.04	8*	33.24	32.66/33.74	33.58/33.35	33.02/33.47	4*
GCNII/ +*	40.61	37.94/43.99	33.24/30.58	28.43/29.66	4*	66.89	54.39/54.69	44.36/48.46	46.49/29.77	2	31.84	24.61/24.67	24.93/26.85	24.47/24.80	2
GPNN/ +*	43.04	27.95/38.74	18.54/29.47	18.54/28.61	2	64.47	50.66/65.55	48.03/52.77	29.39/45.08	4*	24.67	25.00/25.63	24.67/24.88	22.18/25.09	4*
JKNet/ +*	47.36	59.75/61.08	58.69/61.22	57.83/61.48	8*	64.25	70.18/72.37	70.83/69.44	70.61/70.93	4*	28.09	27.17/29.67	27.57/30.04	28.09/29.65	6*
MGNN/ +*	41.79	45.44/48.76	41.31/43.79	39.00/40.28	4*	58.33	64.25/64.79	61.18/62.80	61.40/59.72	4*	30.53	35.99/37.65	35.92/37.23	37.17/37.08	4*
Chameleon ($\mathcal{H}_{node} = 0.23$)															
GCN/ +*	67.11	63.82/63.39	59.65/63.38	57.89/60.31	2	67.11	63.82/63.39	59.65/63.38	57.89/60.31	2	29.98	26.64/25.67	27.50/28.60	26.83/28.22	2
GIN/ +*	66.89	54.39/54.69	44.36/48.46	46.49/29.77	2	66.89	54.39/54.69	44.36/48.46	46.49/29.77	2	31.84	24.61/24.67	24.93/26.85	24.47/24.80	2
GAT/ +*	69.74	70.61/70.83	66.89/66.23	61.84/63.77	4*	69.74	70.61/70.83	66.89/66.23	61.84/63.77	4*	28.09	27.57/27.87	25.26/25.86	25.13/26.58	2
Mixhop/ +*	66.45	64.69/69.08	63.38/66.04	62.67/65.89	4*	66.45	64.69/69.08	63.38/66.04	62.67/65.89	4*	32.63	31.25/34.80	35.72/36.68	35.20/35.28	6*
Geom-GCN/ +*	38.44	36.47/40.33	31.42/38.67	27.00/36.92	4*	60.75	61.42/63.92	55.73/59.12	54.32/58.46	4*	31.59	22.64/32.26	22.64/33.40	22.64/28.21	6*
H2GCN/ +*	27.35	27.94/27.04	30.07/28.21	OOM	6*	55.86	55.92/53.82	53.07/55.24	51.24/56.04	8*	33.24	32.66/33.74	33.58/33.35	33.02/33.47	4*
GCNII/ +*	40.61	37.94/43.99	33.24/30.58	28.43/29.66	4*	66.89	54.39/54.69	44.36/48.46	46.49/29.77	2	31.84	24.61/24.67	24.93/26.85	24.47/24.80	2
GPNN/ +*	43.04	27.95/38.74	18.54/29.47	18.54/28.61	2	64.47	50.66/65.55	48.03/52.77	29.39/45.08	4*	24.67	25.00/25.63	24.67/24.88	22.18/25.09	4*
JKNet/ +*	47.36	59.75/61.08	58.69/61.22	57.83/61.48	8*	64.25	70.18/72.37	70.83/69.44	70.61/70.93	4*	28.09	27.17/29.67	27.57/30.04	28.09/29.65	6*
MGNN/ +*	41.79	45.44/48.76	41.31/43.79	39.00/40.28	4*	58.33	64.25/64.79	61.18/62.80	61.40/59.72	4*	30.53	35.99/37.65	35.92/37.23	37.17/37.08	4*
Actor ($\mathcal{H}_{node} = 0.22$)															
GCN/ +*	55.83	53.51/56.20	51.01/51.87	49.76/53.74	4*	67.11	63.82/63.39	59.65/63.38	57.89/60.31	2	29.98	26.64/25.67	27.50/28.60	26.83/28.22	2
GIN/ +*	46.69	43.26/47.93	43.23/46.89	39.48/44.86	4*	63.82	62.28/66.89	60.31/64.04	58.11/61.62	4*	29.34	29.87/30.83	23.95/25.46	24.41/25.68	4*
GAT/ +*	60.42	46.11/47.55	19.31/28.41	21.33/26.33	2	6									

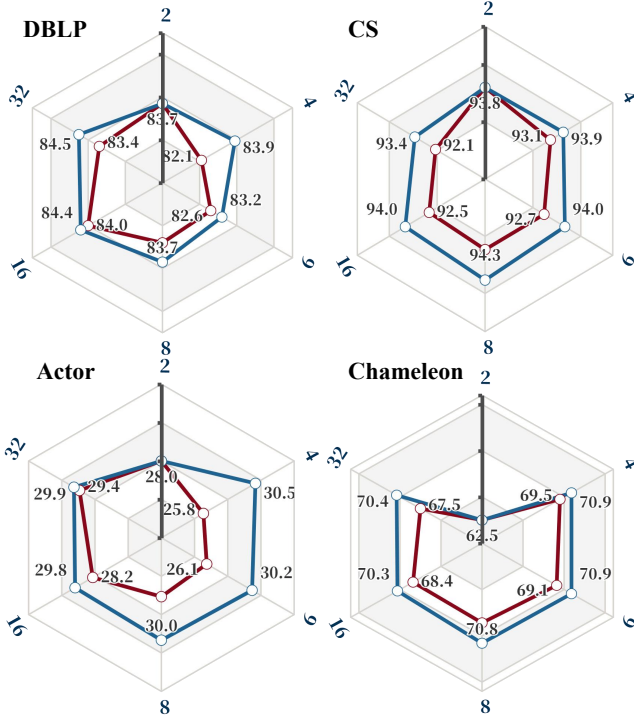


Figure 5: The JKNet and +HES results across CS, DBLP, Actor and Chameleon four benchmarks on 2, 4, 8, 16, 32-layer settings.

5.3 Extend Hetero-S to Deep GNNs (RQ2)

To provide a scalable solution for large and densely connected heterophilic graphs, we extend the HES algorithm to deep GNN contexts. Specifically, we select ResGCN [31], JKNet [65], GCNII [7] and SGC [59] as backbones and conduct tests on 2 homophilic and 2 heterophilic graphs, assessing performance at depths of up to 32 layers. For homophilic graphs, we opt for CS and DBLP [46], whose $\mathcal{H}_{\text{node}}$ is 0.81 and 0.82, respectively. For heterophilic graphs, we choose Actor ($\mathcal{H}_{\text{node}} = 0.22$) and Chameleon ($\mathcal{H}_{\text{node}} = 0.23$). We list the following observations:

Obs.4. Hetero-S consistently boost GNNs at all depths. As illustrated in Figure 5, the blue line represents the enhanced model performance with the addition of HES, while the red line depicts the original baseline. We observed that incorporating the HES algorithm leads to performance gains in both homophilic and heterophilic graph contexts. Notably, for the **Chameleon** dataset, the integration of the HES algorithm resulted in a performance increase of nearly 2.9% against the JKNet baseline.

Obs.5. Hetero-S can assist the “top-student” backbones. An intriguing observation is that JKNet does not exhibit significant performance degradation with the deepening of both homophilic and heterophilic graphs. However, even for the specifically deepened network JKNet, HES still demonstrates exceptional auxiliary performance, further proving the importance of early stopping in receptive fields. We have placed additional experimental results in Appendix E, from which we can draw similar conclusions.

Additionally, the conventional SnoH [53] is specially designed for deepening GNNs on homophilic graphs, and we provide further comparisons between Hetero-S and SnoH in Appendix F.

5.4 Compare With Pruning Methods (RQ3)

In this section, we compare HES with current SOTA pruning methods, UGS [8] and DSpar [4]. We attempt to understand whether Hetero-S can (1) achieve satisfactory sparsity without compromising performance, and (2) genuinely accelerate GNN computations. As shown in Table 2 and Figure 6, we can list the observations:

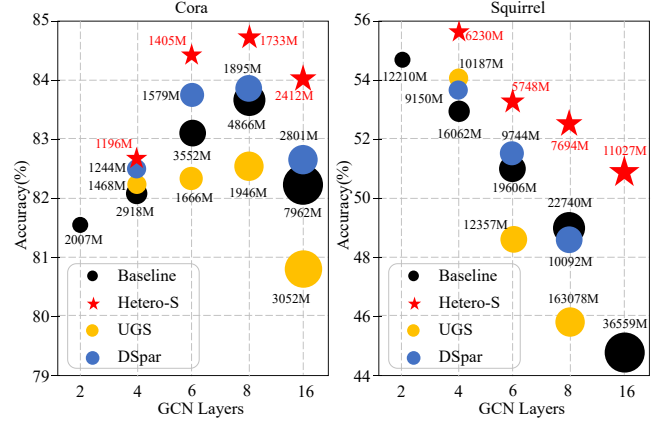


Figure 6: Summary of performance (y-axis) at different graph and GNN layers (x-axis) on Cora and Squirrel. The size of markers represents the inference MACs ($= \frac{1}{2}$ FLOPs) of each sparse GCN on the corresponding sparsified graphs. Black circles (●) indicate the baseline. Blue circles (●) are DSpar. Orange circles (●) represent the UGS. Red stars (★) are established by Hetero-S.

Obs.7. Hetero-S consistently achieves the highest sparsity. As shown in Table 2, with the GNN layers deepening, both UGS and DSpar experience a drastic decline in extreme sparsity. In contrast, Hetero-S demonstrates enhanced sparsity capabilities, surpassing UGS and DSpar by 23.96% and 19.96% on Squirrel+16-layer GCN.

Obs.8. On both datasets, Hetero-S achieved the smallest inference MACs, nearly only 25%-45% of the original baseline. Specifically, on the Cora+16-layer GCN, we observe that Hetero-S can achieve comparable or even better performance than UGS and DSpar, with only 8.04% and 4.89% MACs, respectively. Furthermore, our algorithm consistently improves performance across various GCN depths, especially in deeper layers. Hetero-S surpassed UGS by approximately 2.3%~2.8% on Cora and was able to reliably train 16 layers on Squirrel, outperforming the baseline by nearly 6.2%.

Table 2: The extreme graph sparsity that HES, UGS, and DSpar are capable of achieving, at which GCN suffers no performance degradation compared with the original baseline.

Dataset	Method	2	4	6	8	16
Cora	UGS	18.55	14.26	14.26	9.75	N/A
	DSpar	23.50	21.00	13.00	10.00	7.50
	HES	25.18	28.37	30.75	31.98	34.25
Squirrel	UGS	14.26	9.75	5.00	5.00	N/A
	DSpar	17.00	12.00	7.00	4.00	4.00
	HES	19.11	19.77	20.50	22.89	23.96

5.5 Ablation Study (RQ4)

Since our performance is contingent on the predictive accuracy of the proxy models, we select multiple proxy models to observe the impact of different proxy predictors on the final prediction

results. Concretely, we choose 4-layer GCN and 3-layer GAT, SGC and MLP as proxy predictors to comprehensively verify the model performance. As shown in Table 3, we can make observations:

Table 3: Ablation study on different proxy models.

Dataset	GCN	GAT	SGC	MLP
Cora	82.89 \pm 0.92	82.11 \pm 1.24	82.66 \pm 0.58	82.73 \pm 0.63
Citeseer	73.34 \pm 0.82	72.97 \pm 1.53	73.79 \pm 1.04	73.40 \pm 0.93
Texas	77.41 \pm 3.52	75.81 \pm 4.96	77.64 \pm 2.54	78.95 \pm 2.87
Squirrel	55.58 \pm 1.72	55.16 \pm 1.63	56.17 \pm 1.20	56.20 \pm 1.54
Chameleon	62.97 \pm 0.98	63.96 \pm 1.22	63.08 \pm 0.95	63.39 \pm 0.89
Avg. Rank	2.8	3.4	2.2	1.6

Obs.9. HES Shows limited sensitivity to proxy model selection. Across all five datasets, the performance variance of snowflakes obtained using different proxy models ranged narrowly between 0.78% and 1.31%. Specifically, the overall performance ranking is MLP > SGC > GCN > GAT, so we leverage a 3-layer MLP for the unified experimental setup in all experiments.

6 RELATED WORK

Our research primarily focuses on the domain of GNNs and is highly pertinent to two specific areas. Due to space constraints, we have included the comprehensive related work in the appendix I.

Graph Pooling & Clustering devote to reducing the computational burden of GNNs by applying pruning or compressing methods [6, 8, 13, 13, 19, 54], which are highly relevant to our research. We divide existing techniques into two categories. (1) *Sampling-based methods* aims at selecting the most expressive nodes or edges from the original graph to construct a new subgraph [19, 29, 41, 74]. Though efficient, the dropping of nodes/edges sometimes results in severe information loss and isolated subgraphs, which may cripple the performance of GNNs [60]. (2) *Clustering-based methods* learns how to cluster the whole nodes in the original graph to produce a informative small graph [43, 60, 69], which can remedy the aforementioned information loss problem.

Heterophilic GNNs. Existing heterophilic GNNs primarily fall into two categories: *non-local neighbor extension* and **GNN architecture refinement** [75]. The former emphasizes expanding the neighborhood scope, achieved via high-order neighbor information mixing [3, 26, 58, 79] and potential neighbor discovery [36, 40, 67]. The latter, delves into enhancing GNNs’ expressive power specifically for heterophilic graphs. Strategies include adaptive message aggregation [20, 50], ego-neighbor separation [47, 79], and layer-wise operations [7, 9, 65] to optimize node representation quality. It’s worth emphasizing that our work shares similarities with that of [52], as both approaches utilize proxy models to discern heterogeneity. However, our objective is specifically geared towards pruning the receptive fields that influence aggregation, granting our approach greater versatility. Additionally, our method can better aid in model storage and expedite training.

7 CONCLUSION

In this paper, we first propose the “one node one receptive field” concept in heterophilic graph modeling. We further establish the heterophily snowflake hypothesis philosophy for GNNs. To achieve this, we adopt heterophily-aware early stopping to let certain nodes

have their own receptive fields. In general, we consistently observe “snowflakes” across numerous deep architectures. Furthermore, upon testing virtually every type of heterogenous design, we have discovered that our algorithm adeptly integrates with various frameworks, significantly enhancing their performance.

8 ACKNOWLEDGMENT

This work is in part supported by the Guangzhou-HKUST(GZ) Joint Funding Program (No. 2024A03J0620).

REFERENCES

- [1] Emmanuel Abbe. 2017. Community detection and stochastic block models: recent developments. *The Journal of Machine Learning Research* 18, 1 (2017), 6446–6531.
- [2] Sami Abu-El-Hajja, Amol Kapoor, Bryan Perozzi, and Joonseok Lee. 2020. N-gcn: Multi-scale graph convolution for semi-supervised node classification. In *uncertainty in artificial intelligence*. PMLR, 841–851.
- [3] Sami Abu-El-Hajja, Bryan Perozzi, Amol Kapoor, Nazanin Alipourfard, Kristina Lerman, Hrayr Harutyunyan, Greg Ver Steeg, and Aram Galstyan. 2019. Mixhop: Higher-order graph convolutional architectures via sparsified neighborhood mixing. In *international conference on machine learning*. PMLR, 21–29.
- [4] Anonymous. 2023. Graph Lottery Ticket Automated. In *Submitted to The Twelfth International Conference on Learning Representations*. <https://openreview.net/forum?id=nmBjBZoySX> under review.
- [5] Deli Chen, Yankai Lin, Wei Li, Peng Li, Jie Zhou, and Xu Sun. 2020. Measuring and relieving the over-smoothing problem for graph neural networks from the topological view. In *Proceedings of the AAAI conference on artificial intelligence*, Vol. 34. 3438–3445.
- [6] Jie Chen, Tengfei Ma, and Cao Xiao. 2018. Fastgcn: fast learning with graph convolutional networks via importance sampling. *arXiv preprint arXiv:1801.10247* (2018).
- [7] Ming Chen, Zhewei Wei, Zengfeng Huang, Bolin Ding, and Yaliang Li. 2020. Simple and deep graph convolutional networks. In *International conference on machine learning*. PMLR, 1725–1735.
- [8] Tianlong Chen, Yongduo Sui, Xuxi Chen, Aston Zhang, and Zhangyang Wang. 2021. A unified lottery ticket hypothesis for graph neural networks. In *International Conference on Machine Learning*. PMLR, 1695–1706.
- [9] Eli Chien, Jianhao Peng, Pan Li, and Olgica Milenkovic. 2020. Adaptive universal generalized pagerank graph neural network. *arXiv preprint arXiv:2006.07988* (2020).
- [10] Guanyu Cui and Zhewei Wei. 2023. MGNN: Graph Neural Networks Inspired by Distance Geometry Problem. In *Proceedings of the 29th ACM SIGKDD Conference on Knowledge Discovery and Data Mining*. 335–347.
- [11] Enyan Dai, Shijie Zhou, Zhimeng Guo, and Suhang Wang. 2022. Label-Wise Graph Convolutional Network for Heterophilic Graphs. In *Learning on Graphs Conference*. PMLR, 26–1.
- [12] Simon S Du, Kangcheng Hou, Russ R Salakhutdinov, Barnabas Poczos, Ruosong Wang, and Keyulu Xu. 2019. Graph neural tangent kernel: Fusing graph neural networks with graph kernels. *Advances in neural information processing systems* 32 (2019).
- [13] Talya Eden, Shweta Jain, Ali Pinar, Dana Ron, and C Seshadhri. 2018. Provable and practical approximations for the degree distribution using sublinear graph samples. In *Proceedings of the 2018 World Wide Web Conference*. 449–458.
- [14] Wenqi Fan, Yao Ma, Qing Li, Yuan He, Eric Zhao, Jiliang Tang, and Dawei Yin. 2019. Graph neural networks for social recommendation. In *The world wide web conference*. 417–426.
- [15] Junfeng Fang, Wei Liu, Yuan Gao, Zemin Liu, An Zhang, Xiang Wang, and Xiangnan He. 2023. Evaluating Post-hoc Explanations for Graph Neural Networks via Robustness Analysis. In *Thirty-seventh Conference on Neural Information Processing Systems*. <https://openreview.net/forum?id=eD534mPhAg>
- [16] Junfeng Fang, Xiang Wang, An Zhang, Zemin Liu, Xiangnan He, and Tat-Seng Chua. 2023. Cooperative Explanations of Graph Neural Networks. In *WSDM*. ACM, 616–624.
- [17] Guoji Fu, Peilin Zhao, and Yatao Bian. 2022. *p*-Laplacian Based Graph Neural Networks. In *International Conference on Machine Learning*. PMLR, 6878–6917.
- [18] Thorben Funke and Till Becker. 2019. Stochastic block models: A comparison of variants and inference methods. *PLoS one* 14, 4 (2019), e0215296.
- [19] Hongyang Gao and Shuiwang Ji. 2019. Graph u-nets. In *international conference on machine learning*. PMLR, 2083–2092.
- [20] Johannes Gasteiger, Aleksandar Bojchevski, and Stephan Günnemann. 2018. Predict then propagate: Graph neural networks meet personalized pagerank. *arXiv preprint arXiv:1810.05997* (2018).
- [21] Will Hamilton, Zhitaoying, and Jure Leskovec. 2017. Inductive representation learning on large graphs. *Advances in neural information processing systems* 30 (2017).

- [22] Zijian Hu, Zhengyu Yang, Xuefeng Hu, and Ram Nevatia. 2021. Simple: Similar pseudo label exploitation for semi-supervised classification. In *Proceedings of the IEEE/CVF Conference on Computer Vision and Pattern Recognition*. 15099–15108.
- [23] Wei Huang, Yayong Li, Weitao Du, Jie Yin, Richard Yi Da Xu, Ling Chen, and Miao Zhang. 2021. Towards deepening graph neural networks: A GNTK-based optimization perspective. *arXiv preprint arXiv:2103.03113* (2021).
- [24] Arthur Jacot, Franck Gabriel, and Clément Hongler. 2018. Neural tangent kernel: Convergence and generalization in neural networks. *Advances in neural information processing systems* 31 (2018).
- [25] Weiwei Jiang and Jiayun Luo. 2022. Graph neural network for traffic forecasting: A survey. *Expert Systems with Applications* 207 (2022), 117921.
- [26] Di Jin, Zhizhi Yu, Cuiying Huo, Rui Wang, Xiao Wang, Dongxiao He, and Jiawei Han. 2021. Universal graph convolutional networks. *Advances in Neural Information Processing Systems* 34 (2021), 10654–10664.
- [27] Thomas N Kipf and Max Welling. 2016. Semi-supervised classification with graph convolutional networks. *arXiv preprint arXiv:1609.02907* (2016).
- [28] Boris Knyazev, Graham W Taylor, and Mohamed Amer. 2019. Understanding attention and generalization in graph neural networks. *Advances in neural information processing systems* 32 (2019).
- [29] Junhyun Lee, Inyeop Lee, and Jaewoo Kang. 2019. Self-attention graph pooling. In *International conference on machine learning*. PMLR, 3734–3743.
- [30] Namhoon Lee, Thalaisyasingam Ajanthan, and Philip HS Torr. 2018. Snip: Single-shot network pruning based on connection sensitivity. *arXiv preprint arXiv:1810.02340* (2018).
- [31] Qimai Li, Zhichao Han, and Xiao-Ming Wu. 2018. Deeper insights into graph convolutional networks for semi-supervised learning. In *Thirty-Second AAAI Conference on Artificial Intelligence*.
- [32] Xiang Li, Renyu Zhu, Yao Cheng, Caihua Shan, Siqiang Luo, Dongsheng Li, and Weining Qian. 2022. Finding global homophily in graph neural networks when meeting heterophily. In *International Conference on Machine Learning*. PMLR, 13242–13256.
- [33] Derek Lim, Felix Hohne, Xiuyu Li, Sijia Linda Huang, Vaishnavi Gupta, Omkar Bhalerao, and Ser Nam Lim. 2021. Large scale learning on non-homophilous graphs: New benchmarks and strong simple methods. *Advances in Neural Information Processing Systems* 34 (2021), 20887–20902.
- [34] Derek Lim, Xiuyu Li, Felix Hohne, and Ser-Nam Lim. 2021. New benchmarks for learning on non-homophilous graphs. *arXiv preprint arXiv:2104.01404* (2021).
- [35] Meng Liu, Hongyang Gao, and Shuiwang Ji. 2020. Towards deeper graph neural networks. In *Proceedings of the 26th ACM SIGKDD international conference on knowledge discovery & data mining*. 338–348.
- [36] Meng Liu, Zhengyang Wang, and Shuiwang Ji. 2021. Non-local graph neural networks. *IEEE transactions on pattern analysis and machine intelligence* 44, 12 (2021), 10270–10276.
- [37] Zirui Liu, Kaixiong Zhou, Zhimeng Jiang, Li Li, Rui Chen, Soo-Hyun Choi, and Xia Hu. 2023. DSpar: An Embarrassingly Simple Strategy for Efficient GNN Training and Inference via Degree-Based Sparsification. *Transactions on Machine Learning Research* (2023).
- [38] Sitao Luan, Chenqing Hua, Qincheng Lu, Jiaqi Zhu, Mingde Zhao, Shuyuan Zhang, Xiao-Wen Chang, and Doina Precup. 2022. Revisiting heterophily for graph neural networks. *Advances in neural information processing systems* 35 (2022), 1362–1375.
- [39] Xiaojun Ma, Junshan Wang, Hanyue Chen, and Guojie Song. 2021. Improving graph neural networks with structural adaptive receptive fields. In *Proceedings of the Web Conference 2021*. 2438–2447.
- [40] Hongbin Pei, Bingzhe Wei, Kevin Chen-Chuan Chang, Yu Lei, and Bo Yang. 2020. Geom-gcn: Geometric graph convolutional networks. *arXiv preprint arXiv:2002.05287* (2020).
- [41] Ekagra Ranjan, Soumya Sanyal, and Partha Talukdar. 2020. Asap: Adaptive structure aware pooling for learning hierarchical graph representations. In *Proceedings of the AAAI Conference on Artificial Intelligence*, Vol. 34. 5470–5477.
- [42] Yu Rong, Wenbing Huang, Tingyang Xu, and Junzhou Huang. 2019. Dropedge: Towards deep graph convolutional networks on node classification. *arXiv preprint arXiv:1907.10903* (2019).
- [43] Kashob Kumar Roy, Amit Roy, AKM Mahbubur Rahman, M Ashrafur Amin, and Amin Ahsan Ali. 2021. Structure-Aware Hierarchical Graph Pooling using Information Bottleneck. In *2021 International Joint Conference on Neural Networks (IJCNN)*. IEEE, 1–8.
- [44] Benedek Rozemberczki, Carl Allen, and Rik Sarkar. 2021. Multi-scale attributed node embedding. *Journal of Complex Networks* 9, 2 (2021), cnab014.
- [45] Franco Scarselli, Marco Gori, Ah Chung Tsoi, Markus Hagenbuchner, and Gabriele Monfardini. 2008. The graph neural network model. *IEEE transactions on neural networks* 20, 1 (2008), 61–80.
- [46] Aleksandr Shchur, Maximilian Mumme, Aleksandar Bojchevski, and Stephan Günnemann. 2019. Pitfalls of Graph Neural Network Evaluation. *arXiv:1811.05868* [cs.LG]
- [47] Susheel Suresh, Vinith Budde, Jennifer Neville, Pan Li, and Jianzhu Ma. 2021. Breaking the limit of graph neural networks by improving the assortativity of graphs with local mixing patterns. In *Proceedings of the 27th ACM SIGKDD Conference on Knowledge Discovery & Data Mining*. 1541–1551.
- [48] Kiran K Thekumparampil, Chong Wang, Sewoong Oh, and Li-Jia Li. 2018. Attention-based graph neural network for semi-supervised learning. *arXiv preprint arXiv:1803.03735* (2018).
- [49] Petar Velickovic, Guillem Cucurull, Arantxa Casanova, Adriana Romero, Pietro Lio, and Yoshua Bengio. 2017. Graph attention networks. *stat* 1050 (2017), 20.
- [50] Petar Velickovic, Guillem Cucurull, Arantxa Casanova, Adriana Romero, Pietro Lio, and Yoshua Bengio. 2017. Graph attention networks. *arXiv preprint arXiv:1710.10903* (2017).
- [51] Clement Vignac, Andreas Loukas, and Pascal Frossard. 2020. Building powerful and equivariant graph neural networks with structural message-passing. *Advances in neural information processing systems* 33 (2020), 14143–14155.
- [52] Junfu Wang, Yuanfang Guo, Liang Yang, and Yunhong Wang. 2023. Heterophily-Aware Graph Attention Network. *arXiv preprint arXiv:2302.03228* (2023).
- [53] Kun Wang, Guohao Li, Shilong Wang, Guibin Zhang, Kai Wang, Yang You, Xiaojiang Peng, Yuxuan Liang, and Yang Wang. 2023. The Snowflake Hypothesis: Training Deep GNN with One Node One Receptive field. *arXiv preprint arXiv:2308.10903* (2023).
- [54] Kun Wang, Yuxuan Liang, Xinglin Li, Guohao Li, Bernard Ghanem, Roger Zimmermann, Huahui Yi, Yudong Zhang, Yang Wang, et al. 2023. Brave the Wind and the Waves: Discovering Robust and Generalizable Graph Lottery Tickets. *IEEE Transactions on Pattern Analysis and Machine Intelligence* (2023).
- [55] Kun Wang, Yuxuan Liang, Pengkun Wang, Xu Wang, Pengfei Gu, Junfeng Wang, and Yang Wang. 2022. Searching Lottery Tickets in Graph Neural Networks: A Dual Perspective. In *The Eleventh International Conference on Learning Representations*.
- [56] Kun Wang, Zhengyang Zhou, Xu Wang, Pengkun Wang, Qi Fang, and Yang Wang. 2022. A2DJP: A two graph-based component fused learning framework for urban anomaly distribution and duration joint-prediction. *IEEE Transactions on Knowledge and Data Engineering* (2022).
- [57] Xiao Wang, Houye Ji, Chuan Shi, Bai Wang, Yanfang Ye, Peng Cui, and Philip S Yu. 2019. Heterogeneous graph attention network. In *The world wide web conference*. 2022–2032.
- [58] Yu Wang and Tyler Derr. 2021. Tree decomposed graph neural network. In *Proceedings of the 30th ACM international conference on information & knowledge management*. 2040–2049.
- [59] Felix Wu, Amauri Souza, Tianyi Zhang, Christopher Fifty, Tao Yu, and Kilian Weinberger. 2019. Simplifying graph convolutional networks. In *International conference on machine learning*. PMLR, 6861–6871.
- [60] Junran Wu, Xueyuan Chen, Ke Xu, and Shangzhe Li. 2022. Structural Entropy Guided Graph Hierarchical Pooling. In *International Conference on Machine Learning*. PMLR, 24017–24030.
- [61] Shiwen Wu, Fei Sun, Wentao Zhang, Xu Xie, and Bin Cui. 2022. Graph neural networks in recommender systems: a survey. *Comput. Surveys* 55, 5 (2022), 1–37.
- [62] Shu Wu, Yuyuan Tang, Yanqiao Zhu, Liang Wang, Xing Xie, and Tieniu Tan. 2019. Session-based recommendation with graph neural networks. In *Proceedings of the AAAI conference on artificial intelligence*, Vol. 33. 346–353.
- [63] Zonghan Wu, Shirui Pan, Fengwen Chen, Guodong Long, Chengqi Zhang, and S Yu Philip. 2020. A comprehensive survey on graph neural networks. *IEEE transactions on neural networks and learning systems* 32, 1 (2020), 4–24.
- [64] Keyulu Xu, Weihua Hu, Jure Leskovec, and Stefanie Jegelka. 2018. How powerful are graph neural networks? *arXiv preprint arXiv:1810.00826* (2018).
- [65] Keyulu Xu, Chengtao Li, Yonglong Tian, Tomohiro Sonobe, Ken-ichi Kawarabayashi, and Stefanie Jegelka. 2018. Representation learning on graphs with jumping knowledge networks. In *International conference on machine learning*. PMLR, 5453–5462.
- [66] Yujun Yan, Milad Hashemi, Kevin Swersky, Yaoqing Yang, and Danai Koutra. 2022. Two sides of the same coin: Heterophily and oversmoothing in graph convolutional neural networks. In *2022 IEEE International Conference on Data Mining (ICDM)*. IEEE, 1287–1292.
- [67] Tianmeng Yang, Yujing Wang, Zhihan Yue, Yaming Yang, Yunhai Tong, and Jing Bai. 2022. Graph pointer neural networks. In *Proceedings of the AAAI conference on artificial intelligence*, Vol. 36. 8832–8839.
- [68] Zhitao Ying, Dylan Bourgeois, Jiaxuan You, Marinka Zitnik, and Jure Leskovec. 2019. Gnnexplainer: Generating explanations for graph neural networks. *Advances in neural information processing systems* 32 (2019).
- [69] Zhitao Ying, Jiaxuan You, Christopher Morris, Xiang Ren, Will Hamilton, and Jure Leskovec. 2018. Hierarchical graph representation learning with differentiable pooling. *Advances in neural information processing systems* 31 (2018).
- [70] Jiaxuan You, Rex Ying, and Jure Leskovec. 2019. Position-aware graph neural networks. In *International conference on machine learning*. PMLR, 7134–7143.
- [71] Changqian Yu, Yifan Liu, Changxin Gao, Chunhua Shen, and Nong Sang. 2020. Representative graph neural network. In *Computer Vision—ECCV 2020: 16th European Conference, Glasgow, UK, August 23–28, 2020, Proceedings, Part VII* 16. Springer, 379–396.
- [72] Muhan Zhang and Yixin Chen. 2018. Link prediction based on graph neural networks. *Advances in neural information processing systems* 31 (2018).

- [73] Muhan Zhang and Yixin Chen. 2019. Inductive matrix completion based on graph neural networks. *arXiv preprint arXiv:1904.12058* (2019).
- [74] Zhen Zhang, Jiajun Bu, Martin Ester, Jianfeng Zhang, Zhao Li, Chengwei Yao, Dai Huifen, Zhi Yu, and Can Wang. 2021. Hierarchical multi-view graph pooling with structure learning. *IEEE Transactions on Knowledge and Data Engineering* (2021).
- [75] Xin Zheng, Yixin Liu, Shirui Pan, Miao Zhang, Di Jin, and Philip S Yu. 2022. Graph neural networks for graphs with heterophily: A survey. *arXiv preprint arXiv:2202.07082* (2022).
- [76] Jie Zhou, Ganqu Cui, Shengding Hu, Zhengyan Zhang, Cheng Yang, Zhiyuan Liu, Lifeng Wang, Changcheng Li, and Maosong Sun. 2020. Graph neural networks: A review of methods and applications. *AI open* 1 (2020), 57–81.
- [77] Zhengyang Zhou, Gengyu Lin, Kuo Yang, LEI BAI, Yang Wang, et al. 2022. GRTo: Remediating dynamic graph topology-task discordance via target homophily. In *The Eleventh International Conference on Learning Representations*.
- [78] Jiong Zhu, Ryan A Rossi, Anup Rao, Tung Mai, Nedit Lipka, Nesreen K Ahmed, and Danai Koutra. 2021. Graph neural networks with heterophily. In *Proceedings of the AAAI conference on artificial intelligence*, Vol. 35. 11168–11176.
- [79] Jiong Zhu, Yujun Yan, Lingxiao Zhao, Mark Heimann, Leman Akoglu, and Danai Koutra. 2020. Beyond homophily in graph neural networks: Current limitations and effective designs. *Advances in neural information processing systems* 33 (2020), 7793–7804.
- [80] Rong Zhu, Kun Zhao, Hongxia Yang, Wei Lin, Chang Zhou, Baole Ai, Yong Li, and Jingren Zhou. 2019. Aligraph: A comprehensive graph neural network platform. *arXiv preprint arXiv:1902.08730* (2019).

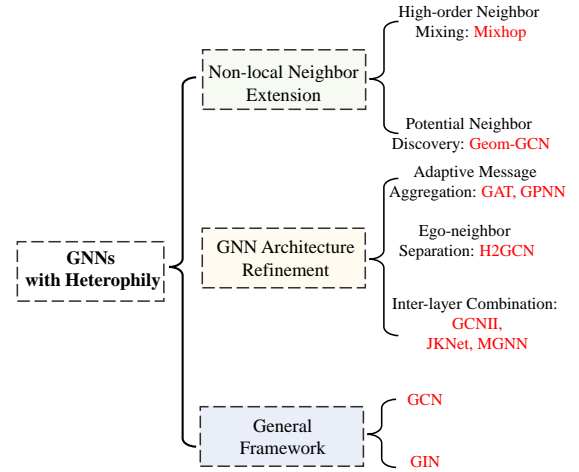


Figure 7: Illustration of backbones adopted in our paper.

A DATASETS AND BACKBONES DESCRIPTIONS.

In this section, we provide a detailed description of the datasets and the backbones to enhance the understanding of our experimental design. The statistical characteristics of the datasets are summarized in Table 4.

Table 4: The statistics of the datasets.

Dataset	#Nodes	#Edges	#Features	#Classes	H_{node}
CiteSeer	3,327	9,104	3,703	6	0.74
PubMed	19,717	88,648	500	3	0.80
CoraFull	19,793	126,842	8,710	70	0.57
DBLP	17,716	105,734	1,639	4	0.82
CS	18,333	163,788	6,805	15	0.81
Cornell	183	557	1,703	5	0.13
Texas	183	574	1,703	5	0.09
Wisconsin	251	916	1,703	5	0.19
Chameleon	2,277	62,792	2,325	5	0.23
Squirrel	5,201	396,846	2,089	5	0.22
Actor	7,600	53,411	932	200	0.22

Backbone Selection for Validation. To systematically validate the capability of our “Heterophily Snowflake Hypothesis,” we have selected 10 backbone architectures. We classify our framework into three main categories: Non-local Neighbor Extension, GNN Architecture Refinement, and General Framework. By summarizing these three categories of work, we can more systematically verify the universality of the “Heterophily Snowflake Hypothesis.” Our model categorization is presented as Figure 7.

High-order Neighbor Mixing. This approach allows nodes to consider neighbors beyond just the immediate, one-hop neighbors. This seems especially beneficial for heterophilic graphs, allowing them to integrate information from nodes that are more than one edge away.

Potential Neighbor Discovery. Instead of just looking at the inherent structure of the graph, this method redefines what a “neighbor” might be. It constructs a potential neighbor set based on some metric function distance in a latent space, rather than just topological closeness.

Adaptive Message Aggregation. Given a set of neighbors, the primary challenge in heterophilic graphs is to effectively aggregate or combine their information. This method seems to alter the aggregation step by weighing the importance of each neighbor differently. The goal is to differentiate information from similar neighbors (of the same class) versus dissimilar neighbors (of different classes).

Ego-Neighbor Separation. The concept of ego-neighbor separation emphasizes differentiating ego node representations from aggregated neighbor nodes for clearer class label distinctions. This approach involves detaching self-loop connections in aggregation and modifying the update function to favor non-mixing operations.

Inter-layer Combination. Inter-layer combination in GNNs diverges from adaptive message aggregation and ego-neighbor separation methods. Instead of focusing on individual layers, it emphasizes layer-wise operations to enhance GNNs’ representation capabilities in heterophily settings. The strategy’s foundation is that while shallow GNN layers capture local information, deeper layers grasp broader, global data through repeated neighbor interactions. In a heterophily context, neighbors having similar data might span both immediate vicinity and distant global structures. Thus, integrating representations from every layer optimally leverages diverse neighbor scopes, considering both localized and broad structural characteristics, leading to more robust heterophilic GNNs.

B ALGORITHM TABLE

C EXPERIMENTAL SETTINGS

In this section, we report our experimental settings according to the research questions.

Algorithm 1: Algorithm workflow of HES

Input : $\mathcal{G} = (\mathbf{A}, \mathbf{X})$, GNN model f_{Θ} , Proxy model \mathcal{P}_Y ,
Epoch number Q , GNN layer count L

- 1 **for** iteration i in $\{1, 2, \dots, Q\}$ **do**
- 2 Forward proxy model and compute $\tilde{\mathbf{Z}} \leftarrow \mathcal{P}_Y(\mathbf{A}, \mathbf{X})$
 / Obtain Homophily mask \mathbf{S} */*
- 3 **for** edge (i, j) in \mathcal{E} **do**
- 4 $S_{ij} \leftarrow \text{trace}(\tilde{z}_i \otimes \tilde{z}_j)$
- 5 Compute k -hop homophily mask $\hat{\mathbf{S}}^{(k)} = \hat{\mathbf{S}}^k \in \mathbb{R}^{N \times N}$
- 6 Compute the row sum of homophily masks
 $\text{set}\{\sum_{\text{row} \setminus \text{diag}} \hat{\mathbf{S}}^{(k)}\} = \{\hat{\mathbf{S}}_1^{(k)}, \hat{\mathbf{S}}_2^{(k)} \dots \hat{\mathbf{S}}_N^{(k)}\}$
- 7 **for** layer l in $\{1, 2, \dots, L\}$ **do**
 / Note that for presentation clarity, we compute
 embeddings for each node individually here. */*
- 8 **for** node v_i in \mathcal{V} **do**
- 9 **if** $\hat{S}_i^{(l)} \leq \rho \hat{S}_i^{(1)}$ **then**
 / Before receptive early stopping */*
 $\mathbf{h}_i^{(l)} \leftarrow$
 $\text{COMB}(\mathbf{h}_i^{(l-1)}, \text{AGGR}\{\mathbf{h}_j^{(l-1)} : v_j \in \mathcal{N}(v_i)\})$
- 10 **else**
 / After receptive early stopping */*
 $\mathbf{h}_i^{(l)} \leftarrow \text{COMB}(\mathbf{h}_i^{(l-1)}, \emptyset)$
- 11
- 12
- 13 Compute loss function Eq. 8 and Eq. 11
- 14 Backward to update GNN f_{Θ} and proxy model \mathcal{P}_Y

- **Main experiments (RQ1).** In this setup, we integrate Hetero-S into mainstream heterophilic GNNs, focusing on non-local neighbor extensions (2 backbones), GNN architecture refinements (6 backbones) and general designs (2 backbones).
- **Depth scalability experiments (RQ2).** We delve into varying depths of GNN architectures. The aim is to determine whether the inclusion of Hetero-S enables these GNNs to maintain or enhance performance as the network goes deeper, avoiding issues like vanishing gradients or over-smoothing.
- **Comparative analysis with traditional Snowflake Hypotheses (RQ3).** Here, we juxtapose Hetero-S with its predecessors, SnoHv1 and SnoHv2, on heterophilic graphs. The experiment is tailored to elucidate if Hetero-S presents a more harmonious alignment with the intricacies of heterophily, potentially leading to better model interpretations and results.
- **Efficiency comparison with pruning algorithms (RQ4).** We compare Hetero-S with current SOTA graph sparsification methods (e.g., UGS [8], SNIP [30], DSpar [37]) with a focus on two key aspects: (1) whether Hetero-S can achieve the desired sparsity without performance compromise, and (2) whether Hetero-S can genuinely accelerate model computations.

D ADDITIONAL RESULTS TO ANSWER RQ1.

In this section, we present additional experiments to answer RQ1. We have included new experimental results for the DBLP dataset and provided further training details for selected datasets.

Table 5: Quantitative prediction results of DBLP benchmark compared to backbones and (+*). The best result is indicated in boldface.

Dataset	Model	2-layer	4-layer	6-layer	8-layer
DBLP	GCN / +*	83.31/-	82.97/ 83.33	82.09/ 83.24	80.57/ 82.98
	GIN / +*	80.65/-	80.27/ 80.33	79.39/ 80.35	77.87/ 79.90
	GAT / +*	82.51/-	82.47/ 82.81	81.59/ 82.69	79.57/ 81.52
	Mixhop / +*	83.42/-	83.68/ 84.05	82.81/ 83.96	81.29/ 83.70
	Geom-GCN / +*	82.46/-	28.37/ 44.84	26.38/ 59.36	19.66/ 59.78
	H2GCN / +*	83.96/-	83.92/ 84.95	83.34/ 83.97	83.22/ 83.68
	GCNII / +*	82.07/-	83.16/ 83.89	83.17/ 83.66	83.36/ 83.87
	APPNP / +*	83.39/-	83.05/ 84.02	82.17/ 83.14	80.65/ 81.62
	JKNet / +*	81.94/-	82.91/ 83.24	82.92/ 83.41	83.11/ 83.62
	MGNN / +*	83.84/-	83.50/ 84.29	82.62/ 83.98	81.10/ 81.56

As shown in Table 5, we list observations (1) Across most backbones, the incorporation of Hetero-S generally improved the prediction results, as seen by the higher scores in the columns with the +*. This showcases the potential benefits of integrating Hetero-S into these architectures. (2) Backbones exhibit varied performance across different layer depths. Notably, certain architectures, such as Geom-GCN, experience significant fluctuations in scores as the layers increase. This suggests that while increased depth might amplify the capabilities of some models, it can be counterproductive for others, particularly for GCNII and JKNet. Intriguingly, we observe that upon incorporating Hetero-S, the backbone’s performance can even revert to optimal levels exhibited by the original few layers, including the 2-layer structure. This strongly validates the heterophily snowflake hypothesis we propose.

We also present the performance curves for tests incorporating Hetero-S with the original backbone. As shown in Table 8, we can observe the test performance curves for traditional backbones and the enhancement achieved by integrating our Hetero-S framework. Each graph plots the accuracy over the number of epochs, divided into two scenarios: one for the original backbone (in red) and one for the backbone with Hetero-S (in blue).

For the Chameleon dataset, when comparing the 4-layer, 6-layer, and 8-layer GAT, GCN, GPNN, and JKNet, we can see a consistent pattern. The addition of Hetero-S generally leads to an improvement in maximum test accuracy across all backbone architectures and depths. This is particularly evident in scenarios where the original backbone has a more volatile or lower accuracy trajectory. For instance, in the 4-layer GAT, the peak accuracy improves from 73.53% to 75.45% with the inclusion of Hetero-S. Similar improvements are observed in 6-layer and 8-layer configurations. The 6-layer GAT sees an increase from 73.67% to 76.22%, and the 8-layer from 85.60% to 86.93%. The GCN models also show enhancement with Hetero-S, albeit with a more significant impact on the 4-layer and 6-layer models than on the 8-layer variant. Meanwhile, the GPNN models reflect a notable benefit from Hetero-S at all depths, with the 4-layer model showing an increase from 67.76% to 68.36%, the 6-layer from 55.29% to 58.24%, and the 8-layer from 54.58% to 57.57%. JKNet architectures display similar trends, with the 4-layer model’s accuracy increasing from 72.59% to 73.49%, the 6-layer from 71.93% to 74.59%, and the 8-layer from 74.19% to 74.37%. These results suggest that Hetero-S provides a consistent and noteworthy

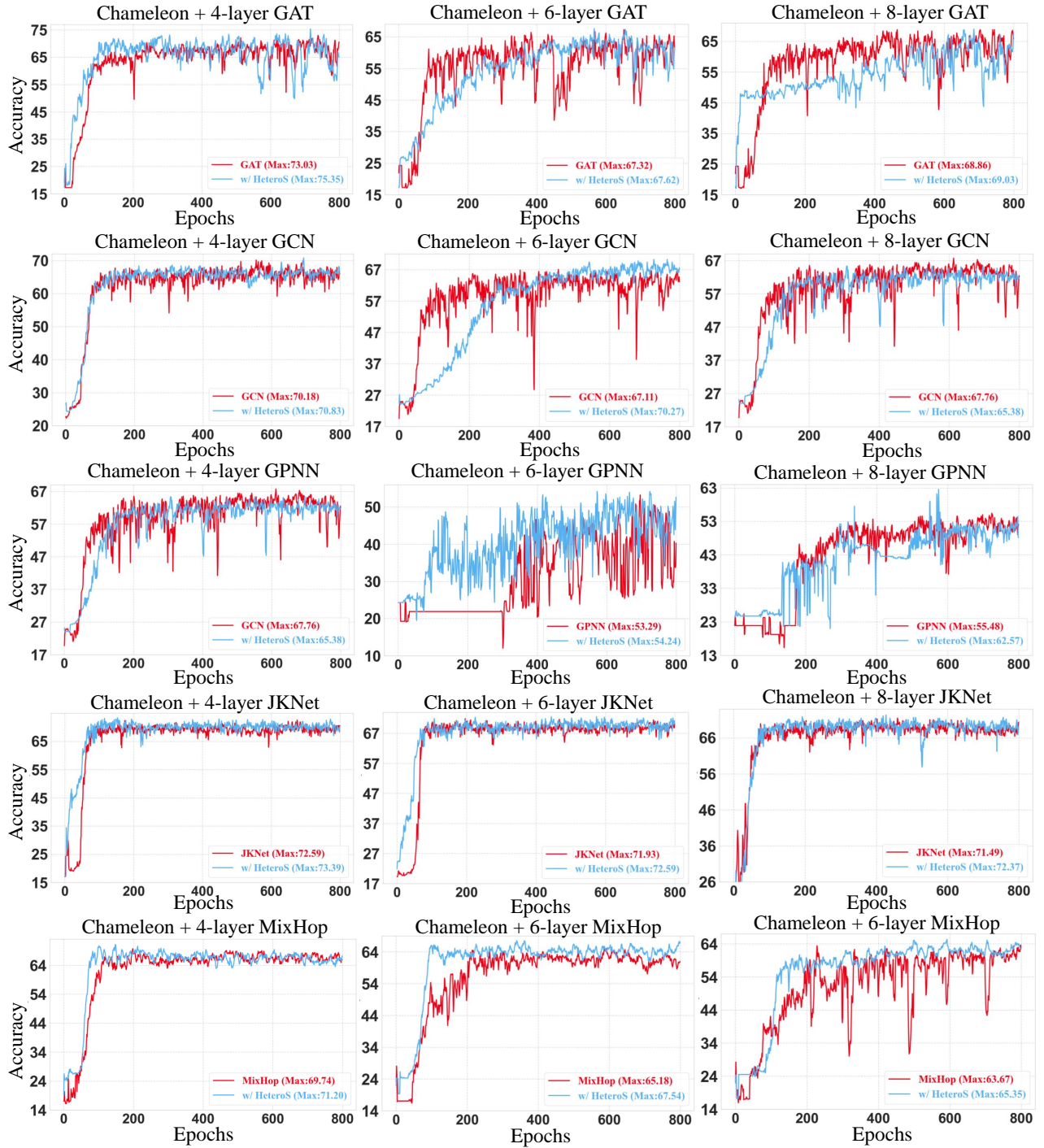


Figure 8: The performance of backbones and the results after adding Hetero-S (+*).

enhancement to the stability and accuracy of various graph neural network architectures across different model complexities. We also showcase more results in Figure 9 ~ 11, from which we can draw similar conclusions from these results.

E ADDITIONAL RESULTS TO SNSWER RQ2.

In this section, we showcase the additional experimental results on DBLP, CS, Chameleon and Actor four graph benchmark. As shown in Figure 12, Incorporating the HES algorithm consistently enhances performance across GCN, GCNII, and SGC models. For example,

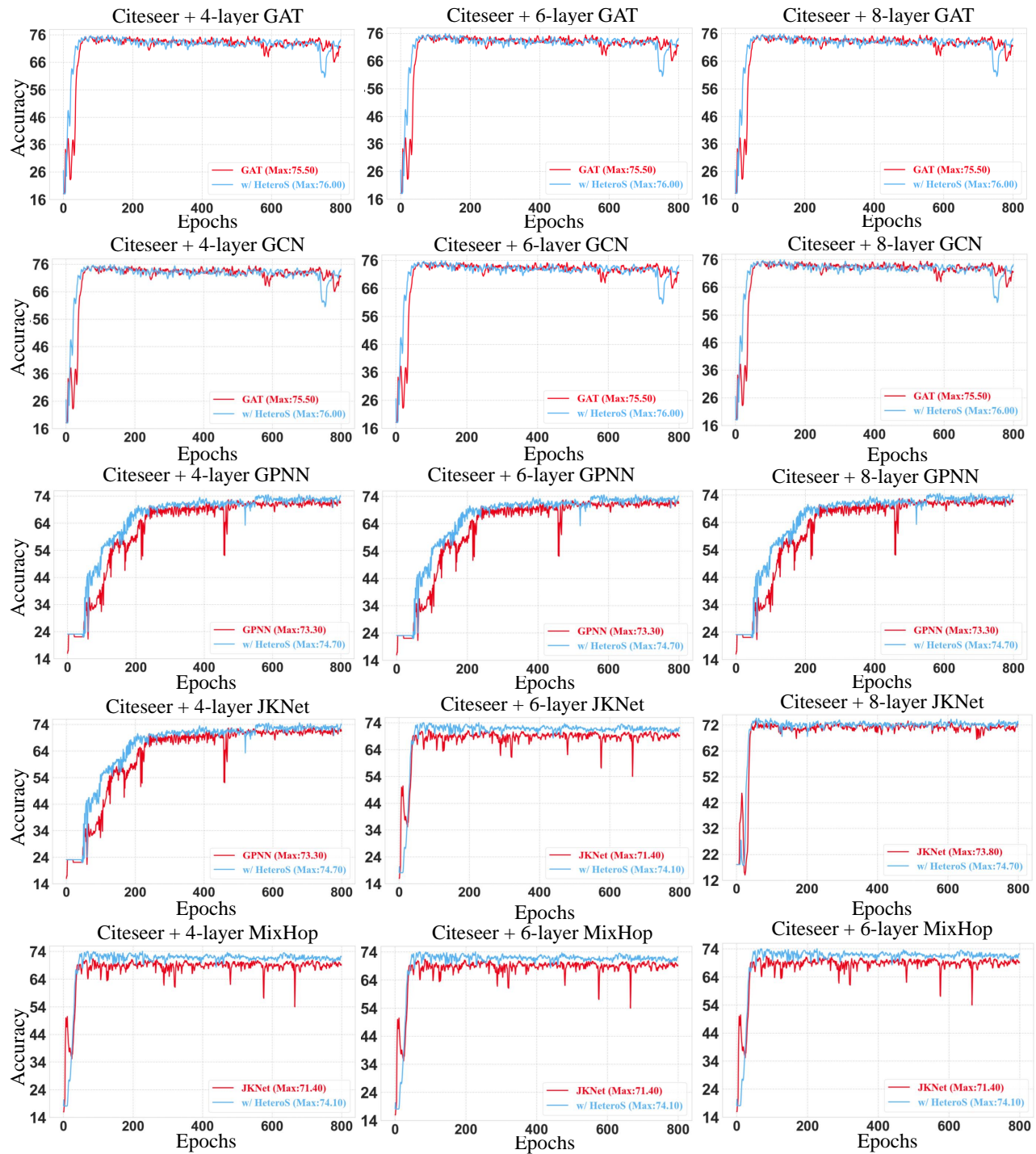


Figure 9: The performance of backbones and the results after adding Hetero-S (+S).

the GCN+DBLP model reveals a significant performance peak at a depth of 8 layers, indicating an optimal balance between model complexity and learning capability. The GCN+CS model consistently performs well, particularly at lower layer counts, suggesting that the HES algorithm captures the essential representational features

efficiently, even without deeper network architectures. Moreover, the GCNII variants benefit more markedly from the integration with the HES algorithm, especially evident in the Actor and Chameleon benchmarks. The enhanced performance indicates that the HES

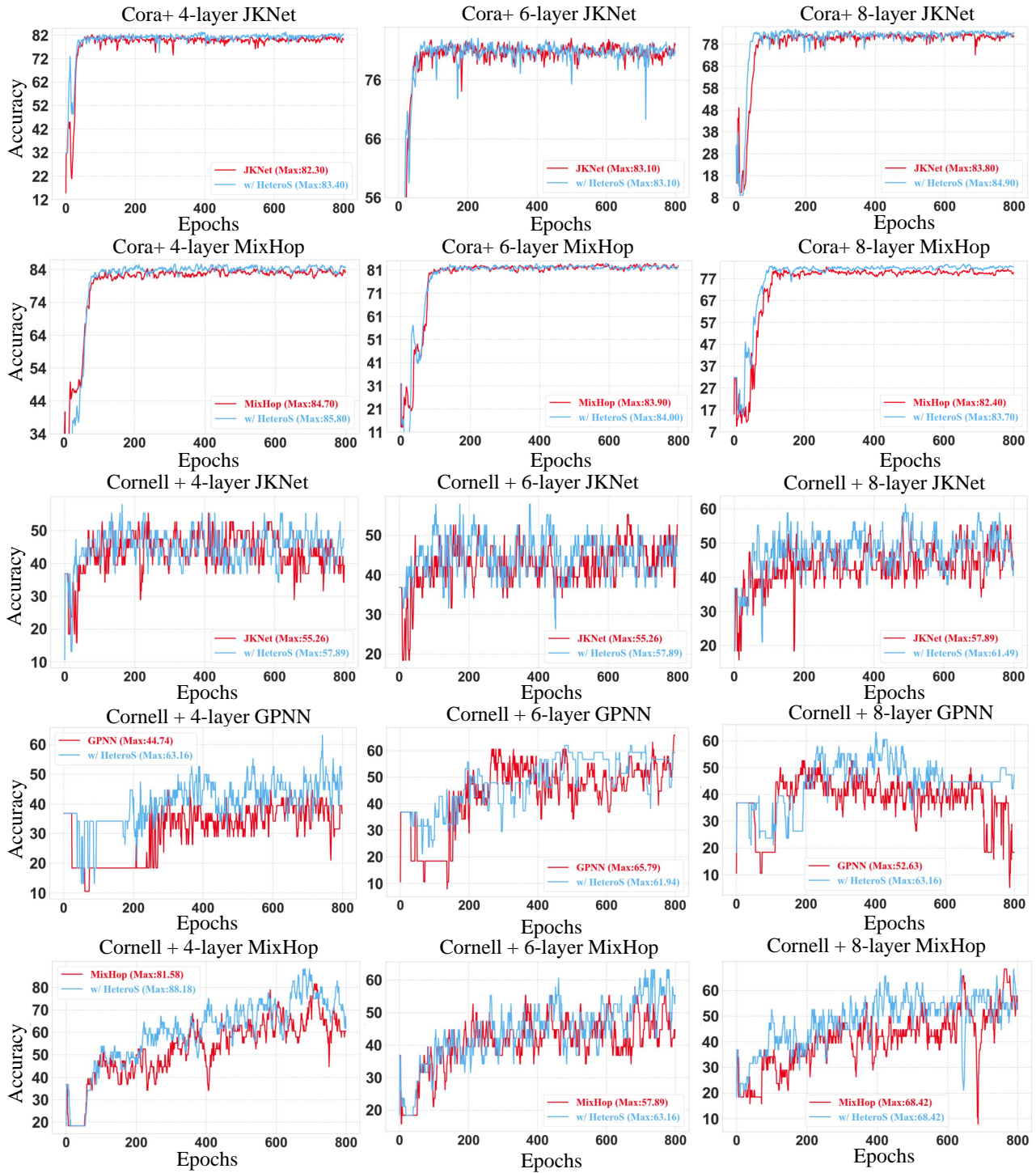


Figure 10: The performance of backbones and the results after adding Hetero-S (+).

algorithm’s approach to leveraging heterogeneity in data aligns exceptionally well with the sophisticated architectures of GCNII.

Furthermore, the SGC models also show improvements in performance, indicating the HES algorithm’s robustness across different

levels of model complexity. This reaffirms its utility as a versatile enhancer of graph network effectiveness. Notably, the performance boosts are not solely dependent on depth but also show a trend of incremental gains with increasing complexity, up to a point where

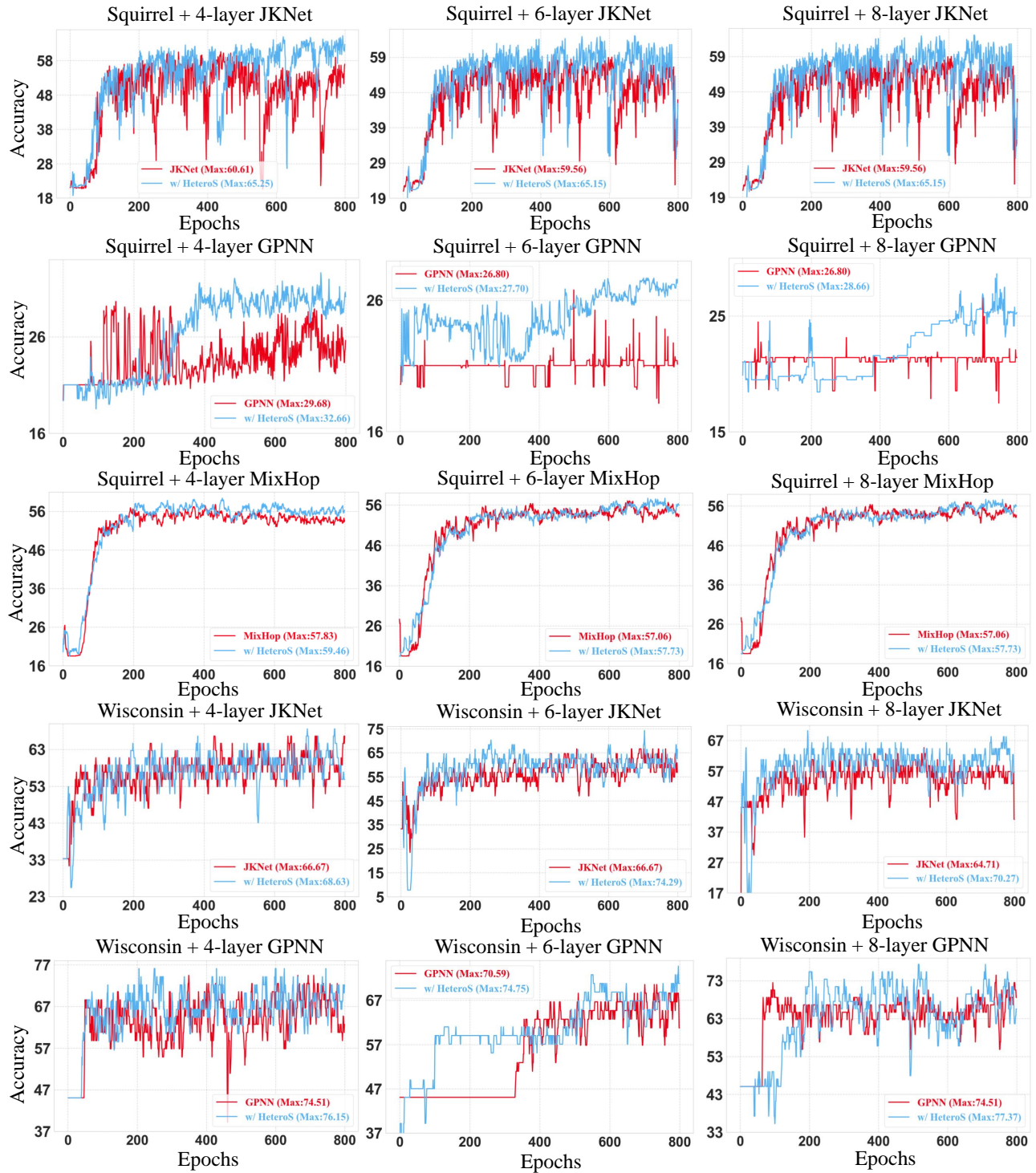


Figure 11: The performance of backbones and the results after adding Hetero-S (+).

performance begins to plateau or slightly decline, highlighting the HES algorithm’s subtle influence on model.

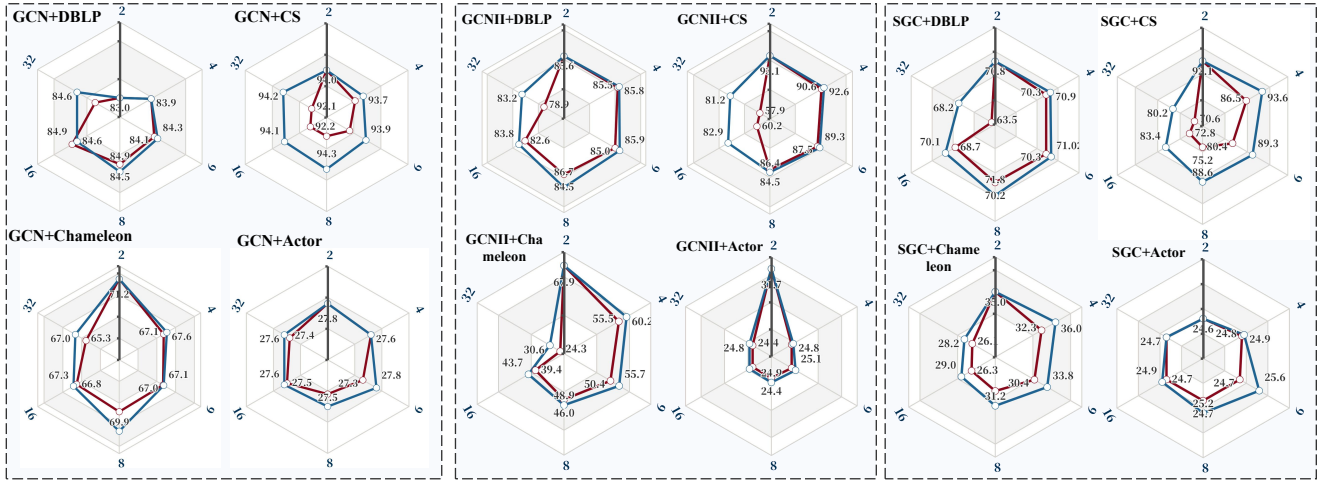


Figure 12: The GCN, GCNII, SGC and Hetero-S results across CS, DBLP, Actor and Chameleon four benchmarks on 2, 4, 8, 16, 32-layer settings.

F PERFORMANCE COMPARISON WITH CONVENTIONAL SNOH

In this section, our focus is on a systematic examination of the performance merits and limitations of HES, in contrast to conventional “snowflake” settings. To facilitate this analysis, we choose six distinct heterophilic graph benchmarks as foundational models for GNNs, specifically: Texas, Wisconsin, Cornell, Squirrel, Chameleon, and Actor. Notably, the depth of heterophilic GNNs is typically observed to not exceed five layers, as indicated by [66]. Hence, within the framework of our heterophilic data approach, we deliberately confine the depth of our network to 6 and 8 layers. This strategic limitation enables us to conduct a thorough and precise comparative analysis of the performances of SnoHv1, SnoHv2, and Hetero-S. In order to conduct a comprehensive comparison, we employ both a homophilic (JkNet) and a heterophilic (Mixhop) GNN as the backbones for our experimental analysis.

Table 6: Comparison results among different “snowflake” methods across 6 and 8-layers under Mixhop backbone setting.

Benchmark (JkNet)	H_{node}	6-layer			8-layer		
		SnoHv1	SnoHv2	Hetero-S	SnoHv1	SnoHv2	Hetero-S
Texas	0.11	82.78 \pm 4.17	83.26 \pm 3.77	84.30 \pm 3.89	86.25 \pm 4.33	86.50 \pm 4.29	89.88 \pm 4.03
Wisconsin	0.21	60.72 \pm 5.88	59.07 \pm 5.12	64.99 \pm 5.05	60.78 \pm 3.93	59.21 \pm 4.20	63.82 \pm 3.51
Cornell	0.22	48.22 \pm 3.87	48.70 \pm 6.85	50.07 \pm 3.25	47.15 \pm 4.28	47.92 \pm 5.04	48.65 \pm 3.98
Squirrel	0.22	59.64 \pm 2.15	58.77 \pm 1.77	61.22 \pm 1.33	59.88 \pm 1.82	59.04 \pm 1.54	61.48 \pm 1.56
Chameleon	0.23	68.93 \pm 1.78	68.56 \pm 2.05	69.44 \pm 1.62	69.42 \pm 2.15	68.77 \pm 2.24	70.93 \pm 1.66
Actor	0.22	28.76 \pm 2.01	28.65 \pm 1.94	30.04 \pm 1.78	28.55 \pm 2.86	27.93 \pm 2.30	29.65 \pm 1.96

Benchmark (MixHop)	H_{node}	6-layer			8-layer		
		SnoHv1	SnoHv2	Hetero-S	SnoHv1	SnoHv2	Hetero-S
Texas	0.11	86.96 \pm 2.88	87.66 \pm 1.79	89.68 \pm 1.43	73.33 \pm 3.80	74.19 \pm 4.65	76.32 \pm 3.17
Wisconsin	0.21	76.92 \pm 4.16	78.45 \pm 3.99	82.93 \pm 3.27	75.48 \pm 3.88	76.66 \pm 3.14	80.28 \pm 3.36
Cornell	0.22	55.88 \pm 3.96	57.40 \pm 3.79	64.32 \pm 3.56	41.31 \pm 3.68	49.63 \pm 3.74	65.70 \pm 3.06
Squirrel	0.22	53.12 \pm 0.87	53.70 \pm 1.29	53.67 \pm 1.33	53.09 \pm 1.26	52.76 \pm 0.73	52.87 \pm 0.96
Chameleon	0.23	63.16 \pm 2.23	64.78 \pm 2.77	66.04 \pm 2.50	62.79 \pm 2.18	63.46 \pm 2.94	65.89 \pm 2.66
Actor	0.22	35.87 \pm 0.94	36.02 \pm 1.08	36.68 \pm 0.66	35.79 \pm 0.98	35.11 \pm 0.91	35.28 \pm 0.79

Obs.6. Hetero-S consistently outperforms the other methods (SnoHv1 and SnoHv2) in most benchmarks for both 6-layer and 8-layer configurations. Particularly in the 8-layer

setting under the MixHop backbone, Hetero-S demonstrates a significant advantage, suggesting that our model scales well with depth and benefits from the MixHop architecture. For instance, in the Texas benchmark, Hetero-S shows a remarkable improvement from 76.32 ± 3.17 to 89.88 ± 4.03 , indicating its robustness in deeper network structures.

G PARAMETER SENSITIVITY ANALYSIS

In this section, we detail how we determine the filtering threshold ρ in all experiments and how ρ influences the performance of HES. In practice, we want to avoid both excessively large ρ , as it could lead to premature removal of too large a receptive field during early stopping, resulting in suboptimal model performance, and excessively small ρ , as they could cause central nodes to absorb too much heterophilic information from multi-hop neighbors. Therefore, we search the most suitable ρ in a limited range $\{1e-2, 1e-4, 1e-6, 1e-8, 1e-16\}$ for all experiments. To further demonstrate how sensitive our method is to ρ , we test the performance of HES on Squirrel/Chameleon with different filtering threshold settings. As shown in Table 7, we can observe (1) the optimal performance of HES requires an appropriate choice of ρ . Generally, as ρ increases, HES’s performance often initially improves (corresponding to increased removal of receptive fields), then declines (corresponding to excessive removal of receptive fields); (2) Overall, HES is relatively insensitive to the choice of ρ . For instance, on GCN, HES performance varies by no more than 1.04% and 1.34%.

H CASE STUDY

In this section, we endeavor to investigate the efficacy of Hetero-S from a micro-perspective through the analysis of two case studies. We choose the superpixel graphs of MNIST [28] and Squirrel as benchmarks to observe the visualized outcomes. As depicted in Figure 13, the following observations can be made:

- **Left.** On the MNIST dataset, we observe that as the depth of the GNN increases, the edges in the black regions are progressively pruned. At the deepest layer, the adjacency matrix aligns precisely with the white regions, capturing the edge information of

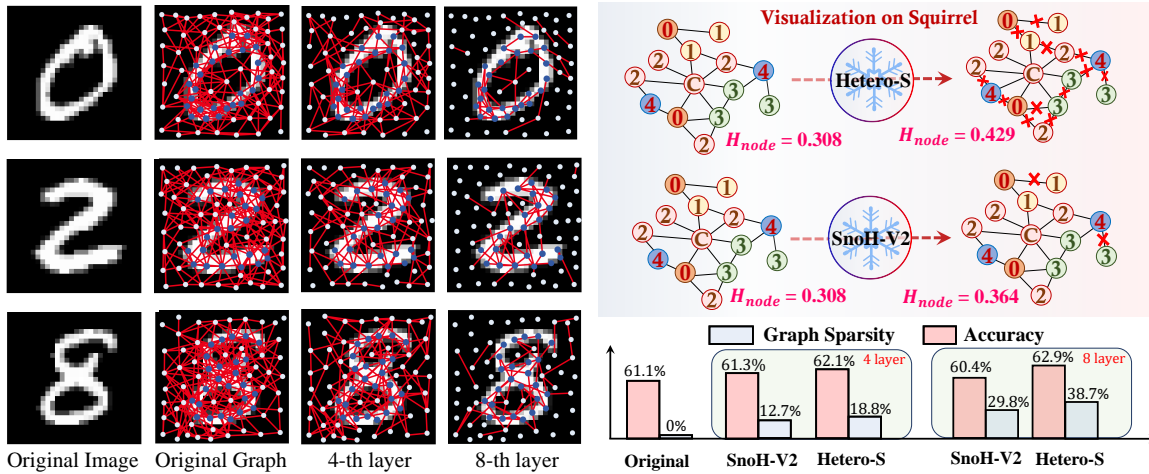


Figure 13: (Left.) Visualization of the subgraphs extracted by applying HES to an 8-layer GCN with MNIST. Original images and graphs are displayed on the first and second columns. Visualization of the subgraphs extracted by applying HES to a 4-layer GCN with Texas. The central (Right.) Prediction results for the central node C (The label is 2) using different algorithms.

Table 7: Parameter sensitivity on filtering threshold ρ . We report the performance with HES under 4-layer settings with different ρ .

Squirrel	1e-2	1e-4	1e-6	1e-8	1e-16
GCN+*	55.18	56.20	55.52	55.78	54.74
MixHop+*	55.42	56.88	55.46	55.20	54.82
JKNet+*	59.77	60.11	60.08	60.02	58.55
MGNN+*	45.65	46.81	47.85	47.23	47.56
Chameleon	1e-2	1e-4	1e-6	1e-8	1e-16
GCN+*	62.25	63.11	63.38	63.23	62.34
MixHop+*	67.74	69.04	68.78	69.08	67.22
JKNet+*	70.17	70.38	72.37	71.69	70.55
MGNN+*	60.19	62.09	61.76	61.92	60.83

the prediction areas, thereby significantly aiding the model’s predictive capability. This validates that the HES algorithm adeptly captures the most critical information for prediction and eliminates redundant information.

- **Right.** In our analysis of the Squirrel, we find that the conventional SnoHv2, after pruning, increases its homophily ratio from 0.308 to 0.364. Conversely, Hetero-S enhances this ratio to 0.429, proving that the *Hetero-S scheme improves the model’s likelihood of aggregating similar labels, thereby boosting the effectiveness of information aggregation.* Hetero-S achieves a dual victory of greater graph sparsity and accuracy compared to SnoH-v2, further attesting to the superior capabilities of HES over SnoH-v2 in heterophilic graph scenarios. For instance, HES consistently surpasses SnoH-v2 by substantial performance margins across Squirrel dataset (0.8% ~ 2.5% \uparrow on accuracy and 6.1% ~ 8.9% \uparrow on graph sparsity).

I RELATED WORK

Graph Neural Networks (GNNs). GNNs have emerged as a prominent subfield in machine learning, specifically tailored to manage and analyze graph-structured data [45, 63]. In general, GNNs owe

their efficacy to a distinct “message-passing” mechanism, which seamlessly integrates topological structures with node characteristics to yield richer graph representations. This process is best described by the mathematical expression $H^{(k)} = M(A, H^{(k-1)}, \theta^{(k)})$. In this equation, $H^{(k)}$ stands for the node embedding after k iterations of GNN aggregation. Meanwhile, M represents the message propagation function, and $\theta^{(k)}$ denotes the trainable parameters at a given layer [14, 35, 64]. The escalating enthusiasm surrounding GNNs has catalyzed the development of a myriad of propagation techniques [25, 68, 80] and model variants [48, 55, 70, 71], which have significantly broadened the arsenal of tools available for graph-oriented learning and exploration.

Graph Pooling & Clustering. Graph pooling and clustering devote to reducing the computational burden of GNNs by applying pruning or compressing methods [6, 8, 8, 13, 13, 19], which are highly relevant to our research. We divide existing techniques into two categories. (1) *Sampling-based methods* aims at selecting the most expressive nodes or edges from the original graph to construct a new subgraph [19, 29, 41, 74]. Though efficient, the dropping of nodes/edges sometimes results in severe information loss and isolated subgraphs, which may cripple the performance of GNNs [60]. (2) *Clustering-based methods* learns how to cluster the whole nodes in the original graph, and produces a informative graph where the clusters are node sets [43, 60, 69], which can remedy the aforementioned information loss problem.

Heterophilic GNNs. Existing heterophilic GNNs primarily fall into two categories: *non-local neighbor extension* and *GNN architecture refinement* [75]. The former emphasizes expanding the neighborhood scope, achieved via high-order neighbor information mixing [3, 26, 58, 79] and potential neighbor discovery [36, 40, 67]. The latter, delves into enhancing GNNs’ expressive power specifically for heterophilic graphs. Strategies include adaptive message aggregation [20, 50], ego-neighbor separation [47, 79], and layer-wise operations [7, 9, 65] to optimize node representation quality.

It's worth emphasizing that our work shares similarities with that of [52], as both approaches utilize proxy models to discern heterogeneity. However, our objective is specifically geared towards pruning the receptive fields that influence aggregation, granting our approach greater versatility. Additionally, our method can better aid in model storage and expedite training.

J PROOF

In this subsection, we present a detailed proof. The notation $\mathbb{E}_{A \sim SBM(p,q)}[\cdot]$ represents the expected pattern of the adjacency matrix. As depicted in main part, considering in subsequent layers, the HES algorithm is applied such that p remains constant while heterophilic nodes are pruned, thus reducing q , the product of the smallest eigenvalues of $\mathbb{E}_{A \sim \psi(N,p,q)}[G]$ is given by:

$$\prod_{i=1}^L \frac{1 - p^{(i)}}{(N-1)p^{(i)} + Nq^{(i)} + 1} = \prod_{i=1}^L \left(1 - \frac{N(p^{(i)} + q^{(i)})}{(1 - p^{(i)}) + N(p^{(i)} + q^{(i)})} \right) \quad (18)$$

Consider the case $p > q$ are both functions of N, i , and suppose $p = 1/((N-1)*i^2)$, $q = 1/(N*i^2)$. In this scenario, as the layer depth increases, both p and q undergo decay, yet maintain the condition $p > q$. Consequently, the product of the smallest eigenvalues can be expressed as:

$$\Psi(L) = \prod_{i=1}^L \frac{(N-1)i^2 - 1}{(N-1)i^2 + 2(N-1)} \quad (19)$$

While the network goes infinitely deep, *a.k.a.* $L \rightarrow \infty$, the infinite product of the smallest eigenvalues can be calculated as follows:

$$\begin{aligned} \Psi(L) &= \prod_{i=1}^L \frac{(N-1)i^2 - 1}{(N-1)(i^2 + 2)} \\ &= \sqrt{2\pi} \operatorname{csch}(\sqrt{2\pi}) \left(1 - \frac{1}{\sqrt{N-1}}\right)_L \left(1 + \frac{1}{\sqrt{N-1}}\right)_L \frac{1}{\Gamma(L - i\sqrt{2} + 1)\Gamma(L + i\sqrt{2} + 1)} \\ &\approx \sqrt{2N} \operatorname{csch}(\sqrt{2\pi}) \sin(\pi/\sqrt{N}) \end{aligned} \quad (20)$$

where $\operatorname{csch}(\cdot)$ denotes the hyperbolic cosecant function, $\Gamma(\cdot)$ denotes the Gamma function and $(a)_L = a(a+1)\dots(a+L-1)$ denotes the Pochhammer Symbol. When the network goes infinitely deep, the value of the infinite product asymptotically approaches a non-zero value $\sqrt{2N} \operatorname{csch}(\sqrt{2\pi}) \sin(\pi/\sqrt{N})$, which concludes the proof.

We posit that this phenomenon is not solely confined to binary classification contexts. Even in multi-class scenarios, a similar pattern is observed. Utilizing the HES algorithm, we can adeptly facilitate the divergence of the GNTK, as opposed to its convergence to zero, thereby enhancing the efficacy of network training.